Universiteit Utrecht

Opleiding Natuur- en Sterrenkunde

Feasibility study of intrinsic charm measurement with ALICE at CERN Large Hadron Collider

Bachelor Thesis

Mahircan Erciyas

Supervisors:

Dr. Alessandro Grelli
Insitute for Subatomic Physics (SAP) at Utrecht University

Dr. Henrique José Correia Zanoli
Insitute for Subatomic Physics (SAP) at Utrecht University

June 16, 2021

Abstract

Quantum ChromoDynamics (QCD) predicts that the proton can have up to five valence quarks, with the additional quark-antiquark pair being an intrinsic component. It is expected that, with a probability in the order of one percentage, the two additional intrinsic quarks can be charm quarks. This is explained by non-perturbative QCD. Previous research shows that this component is expected to overtake perturbative contributions at higher Bjorken x. Although relevant for testing QCD, the study of intrinsic charm is also important to correctly model the background in the discovery measurement of astronomical neutrinos performed by the IceCube Collaboration. In this thesis, a topology involving a central gluon jet, a central D meson, and a forward muon from heavy-flavour hadron decays is proposed as a viable measurement strategy, and simulated whilst keeping in mind the ALICE detector acceptance. To do this, C++ framework ROOT is used along with Pythia8 and LHAPDF6 to simulate five different parton distribution functions (PDF) with varying levels of intrinsic charm, and compared to a PDF set with no intrinsic charm by means of ratios. The results of these simulations show that the proposed topology works in tagging intrinsic charm events. In particular, it is possible, by tuning the transverse momentum (p_T) range of the D meson, to enhance the intrinsic charm contribution of the intermediate muon p_T, allowing one to separate this contribution from the one of the perturbative charm production. This indicates that forward muons are a promising candidate for an intrinsic charm trigger once produced in association with a D meson at central rapidity.

Contents

1 Introduction **1**

2 Background information **3**
2.1 Quantum chromodynamics (QCD) 3
2.2 Intrinsic charm (IC) 4
2.3 Neutrinos and IceCube 5

3 Methodology **6**
3.1 Experimental setup 6
3.1.1 ALICE 6
3.2 Topology 8
3.2.1 D meson 8
3.2.2 Gluon jet 9
3.2.3 Muon from heavy-flavour particle decay 9
3.3 Simulation setup 9
3.3.1 ROOT 10
3.3.2 Pythia8 10
3.3.3 LHAPDF6 13

4 Results and discussion **15**

5 Conclusions and future outlook **31**

6 Laymen summary **33**

1 Introduction

We describe the strong force that governs the formation of subatomic particles using the Standard Model of particle physics. The strong force governs the interactions of quarks and gluons. It is described by Quantum Chromodynamics (QCD), which is a quantum field theory. In QCD, the charm quark production can be described in a perturbative manner via pair creation, gluon splitting and flavour excitation. That being said, it is expected that there is a small non-perturbative contribution as well. This non-perturbative contribution is the so-called intrinsic charm (IC)

Previous work has resulted in several existing models that describe this intrinsic charm component. The original formulation is the BHPS model, which expresses IC as a component of the proton wavefunction which is acquired through so-called Fock space decomposition. This component is that of a proton with an additional charm anti-charm pair acting as valence quarks, i.e. $uudc\bar{c}$. The BHPS model expresses this component as a non-negligible probability function. Another available model is the so-called SEA model, which expresses IC as derived from an additional gluon component in the proton. This gluon component forms an aptly-named quark sea, which encompasses the additional charm production of the SEA model. The common trait of these models is that they contain some non-perturbative component, and become prevalent compared to perturbative production at higher Bjorken x fractions, which correspond to a higher pseudo-rapidity (measure of the angle between the proton beam and outgoing particle, with $\eta = 0$ implying a perpendicular trajectory of the outgoing particle, and $\eta = \infty$ implying a parallel trajectory) values for the produced particles in collisions at TeV energy scale. It is clearly of major importance to be able to experimentally measure the IC fraction (probability) in the proton as a QCD test tool.

Moreover, the importance of IC extends beyond particle physics. Namely, one of the results of the IceCube collaboration was the detection of astronomical neutrinos. These are known to be expelled by cosmic objects such as, for example, supernovae. Such neutrinos are believed to travel in straight paths from the source to our planet, with a minimal probability of being absorbed during the travel since they interact only weakly. Moreover, their energy shape carries information on the energy scale of the event that generated them. Therefore, astronomical neutrinos are of fundamental importance for the study of high-energetic cosmic events. However, the IceCube results include a certain amount of background. The main sources of this background are neutrinos that are produced by charm particle decays within our own atmosphere, the so-called atmospheric neutrinos. The energy shape of the atmospheric neutrinos is almost identical to the one of astronomical neutrinos, and is thus impossible to be separated by means of a standard data analysis. Therefore, the atmospheric neutrino background can only be modelled by means of simulations. The average atmospheric collision is extremely forward and on the multi-TeV energy scale. Such a configuration is exactly where we expect the maximum effect of IC on charm particle production. Therefore, in order to properly model the background of atmospheric neutrinos that stem from charm particle decays, it is mandatory to measure the intrinsic charm component in the proton.

In this thesis, we investigate the possibility to perform the direct measurement of the IC

component in the proton by using the ALICE detector of the CERN Large Hadron Collider (LHC). To pursue our goal, we propose a novel topology as a measurement tool. To do this, we simulate high-energy proton-proton collisions at a center-of-mass energy of 13 TeV using several different parton distribution functions (PDF, a probability density which is a function of the partons' longitudinal momentum fraction obtained by fitting to experimental data. Here, the partons are point-like constituents of hadrons, e.g. charm-quarks) with varying degrees of IC, and compare them to a PDF without any IC. These simulations are performed at the same center-of-mass energy of the data that ALICE will collect. In addition, the experiment's geometrical acceptance is accounted for. The topology we study is comprised of the associate production of a D meson and a gluon jet, back-to-back at central rapidity ($|\eta| < 0.9$), with the addition of a muon from charm particle decays at forward rapidity ($2.5 < y < 4.0$). More details with regards to this topology and setup are included in section 3.1.1.

The next chapter of this thesis starts with a discussion of the theoretical framework surrounding QCD and IC. Subsequently, we discuss atmospheric and astronomical neutrinos and the implications for IceCube. Then, we consider the different regions of the ALICE detector, and to what extent there will be a disparity in the amount of data of the actual experiment compared to that of the simulation. Following that, the different tools and PDFs used for the simulations are explained. Finally, the results are presented and discussed, and a conclusion is drawn.

2 Background information

2.1 Quantum chromodynamics (QCD)

As stated previously, QCD gives a description of the strong force which governs quark and gluon interactions. Much like the fine-structure constant α in QED, there is a coupling constant in QCD which is usually denoted α_s. In QED, this coupling constant decreases as one takes more distance (i.e. lower energy) from a charge carrier due to so-called charge screening. As a result, the effective charge of any charged particle decreases. The concept behind this is that virtual lepton-antilepton pairs are produced within the polarized vacuum surrounding a charged particle, and the virtual lepton with a charge opposing that of the charged particle will tend towards the direction of the particle, whereas the other virtual lepton will tend away from it. This effect 'screens' the charge, making its absolute value smaller.

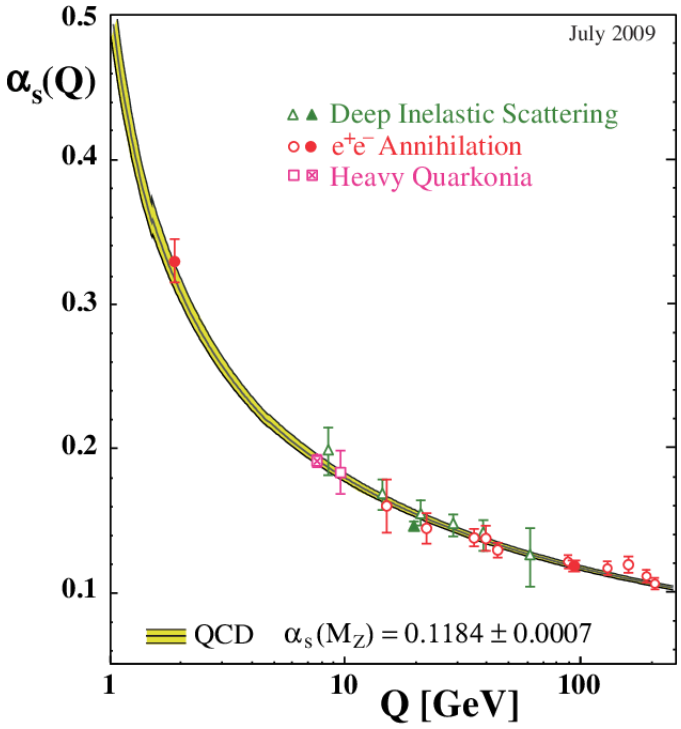

Figure 1: The strong coupling constant (α_s) as a function of the momentum transfer (Q).[1]

In QCD, something similar happens. The main difference in QCD is that the screening is carried out by colour charge rather than electric charge. However, this changes the way the screening functions dramatically, particularly because this effect can be carried out by $q\bar{q}$-pairs, but also gluons. Indeed, because gluons carry both a colour and an anti-colour charge, the screening in QCD effectively augments the effective colour charge rather than diminishing it. In effect, the QCD constant increases with distance rather than decreasing, because the screening augments the charge more and more with larger distances (i.e. lower energies). This vanishing of the QCD constant at extremely high energy scales is called asymptotic freedom, and the screening effect associated with it is called anti-screening.[2]

Within the framework of QCD, the production of pairs of heavy quarks is usually described in a perturbative (pQCD) manner. This method is characterized by higher energies, higher momentum transfers, and subsequently lower length and time scales. In particular the structure of a proton, which is often studied using high-energy deep inelastic scattering (DIS) processes, can be described with pQCD within this context. This is the case because, at these energy levels, the coupling constant α_s becomes so small that one can apply perturbative methods to it. In fact, in DIS processes, α_s is so low that the asymptotic freedom is readily observable; quarks start acting like free particles. However, because a cross section is the result of a combination of both long-distance and short-distance effects, one is generally unable to determine a general cross section using just pQCD. Due to this, methods to separate the long-distance and short-distance contributions, like factorization, have been developed to make certain problems solvable.[3]

The structure of a proton, and even the production of $c\bar{c}$-pairs, can be described in this perturbative manner. In this process, one evaluates the cross section as a function of the coupling constant evaluated at a specific momentum transfer Q^2, which is called the renormalization scale. Using this method to study the proton structure yields methods of $c\bar{c}$-pair production relying on, for example, electron-gluon interactions, or gluon fusion (See figure 2).[4]

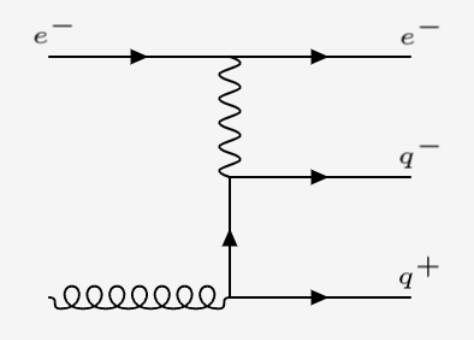

Figure 2: Example of a $ge^- \rightarrow e^-q^-q^+$ process that can be described with pCQD. This is a process that can produce a $c\bar{c}$-pair perturbatively.

2.2 Intrinsic charm (IC)

As opposed to pQCD, where one relies on asymptotic freedom to make calculations in contexts with short length and time scales, there is also non-perturbative QCD, which one must apply when these scales get sufficiently large. There are, in fact, existing calculations that have been made using a technique known as Fock space decomposition. The full explanation of this technique goes beyond the scope of this thesis. However, its notable feature is that one can decompose a wave function (in this case, that of a proton) into individual states involving a specific amount of partons. This allows one to calculate functions describing the specific components $|uudg\rangle$, $|uudb\bar{b}\rangle$, $|uudc\bar{c}\rangle$, etc.

As stated, one of the most notable features of these intrinsic components is that they persist over longer time scales, giving them their non-perturbative nature. However, there is one other particularly notable feature about the states containing an extra valence quark-pair, which is that the heavy quarks within the state carry the majority of the momentum. This follows quite naturally from the fact that these intrinsic components describe bound states, implying that all constituents must be moving with the same velocity. However, it is paramount to the investigation of IC. Namely, perturbative charm-pair production tends to peak at very low momentum fractions of the charm quarks (near a Bjorken x of 0), and fall off significantly at higher ones. This means that intrinsic components are expected to overtake perturbative components as momentum fractions increase (See section 3.3.3). Consequently, the measurement of IC is fundamental in order to validate QCD in this non-perturbative region.[5]

IC can be modelled in different ways, with the functions used in this thesis being based on the Brodsky-Hoyer-Peterson-Sakai (BHPS) model, and the SEA model. With the BHPS model, IC stems directly from the Fock component $|uudc\bar{c}\rangle$, which one can calculate to acquire a probability density function, and subsequently normalize to add a desired percentage of IC to the system. As opposed to this, the SEA model functions by adding a gluon distribution to the existing parton distributions of a proton, allowing the production of additional $q\bar{q}$-pairs from this gluon and resulting in a so-called quark sea.[6][7]

2.3 Neutrinos and IceCube

The measurement of IC is of great importance for the results of the IceCube collaboration. IceCube is a neutrino detector which seeks to acquire data from intergalactic neutrinos expelled by cosmic objects such as supernovae. These neutrinos move through space mostly unperturbed, and thus serve as excellent probes to study faraway cosmic events. However, this comes at a cost, namely that any other neutrinos will cause an additional background underlying the desired data. In IceCube's case, the main source of these background neutrinos are neutrinos that come from charm hadron decays. Such charm particles are produced in high-energy collisions of cosmic rays with the Earth's atmosphere. This background source is usually referred to as atmospheric neutrinos.

Most notably, if the charm production were to be fully understood, then one could just use Monte Carlo generators to simulate and subsequently subtract the contribution of atmospheric neutrinos. However, as explained in section 1, the non-perturbative part of the production (namely the IC) has never been measured. Indeed, the presence of IC at its maximum theoretical values can increase the observed neutrino flux in the astrophysical region by roughly 60%, making it fundamental to have a precise determination of the probability of IC within the proton.[8][9]

3 Methodology

3.1 Experimental setup

3.1.1 ALICE

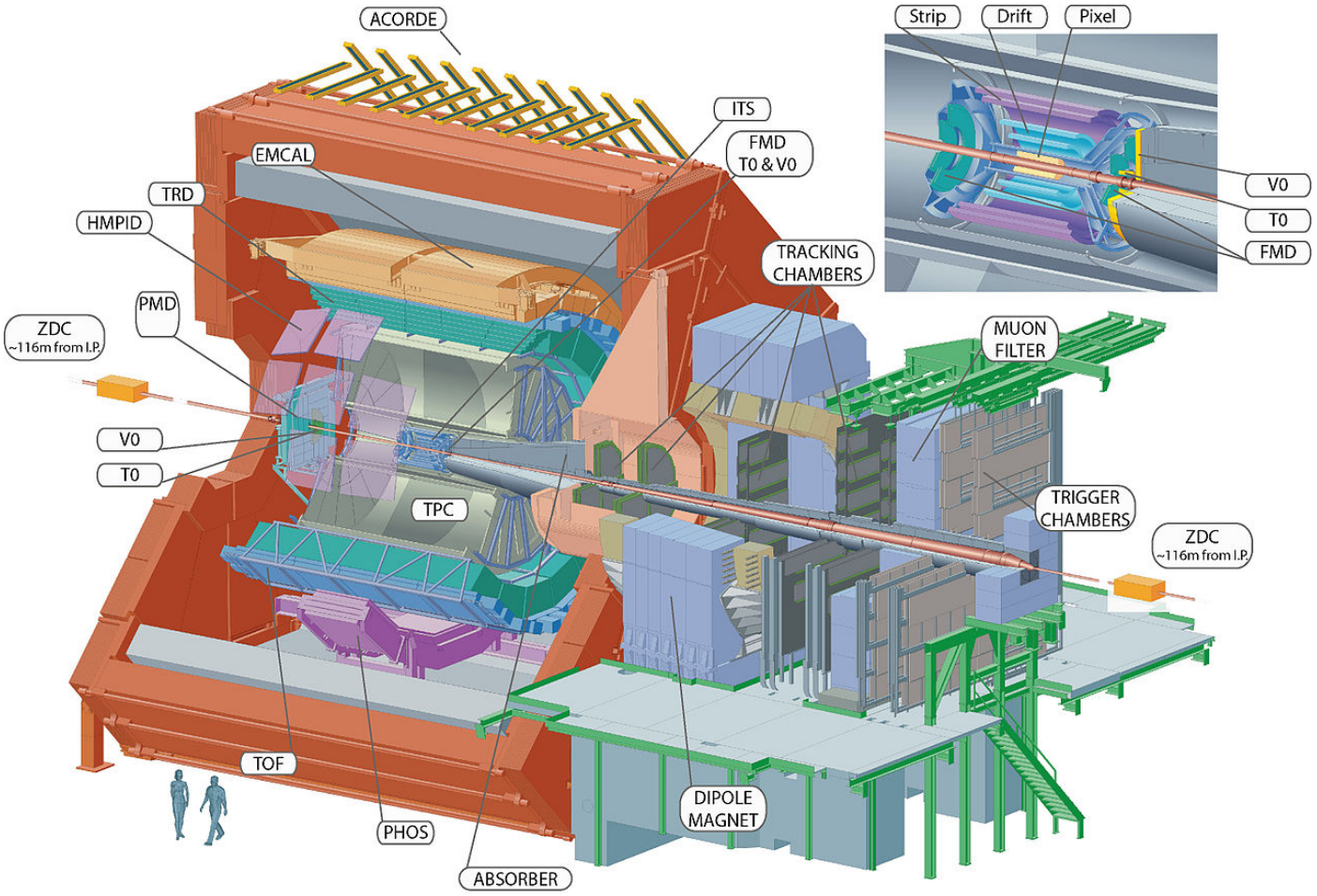

Figure 3: Schematic picture of the ALICE detector.

The Large Hadron Collider (LHC) in Geneva, Switzerland has a total of seven detectors along its circular structure. The relevant detector for this specific project is the ALICE detector (Displayed in Fig. 3). Although the main purpose of the detector is the detection of particles in heavy-ion collisions, it is also used for the study of data of high-energy proton-proton collisions. To do this, it is fitted with various subsystems made to detect specific particles. As explained in section 1, in order to investigate the possible presence of IC, we need to reconstruct gluon jets, D mesons and muons from charm hadron decays. While the muons, due to their relatively long lifetime, can be directly detected by ALICE, for the D mesons, ALICE will detect only their decay products (kaons and pions). Subsequently, the D mesons' reconstruction will proceed by means of invariant mass analysis. Finally, the jets in ALICE will be reconstructed as collimated sprays of charged particles. The subsystems

relevant for this project are as follows.

The time projection chamber (TPC) is a large chamber filled with gas, which uses the ionizing properties of the particles flying through it to detect them. In particular, the chamber contains a Ne-CO_2-N_2 gas mixture which is ionized by charged particles, after which the ionized gas is subject to an electric field running through the chamber, forcing it to the endplates and allowing one to measure the arrival time and reconstruct the trajectory of the ionizing particle using the readout chambers behind the endplates.[10] During long shutdown 2 (LS2), the TPC will be upgraded to work with gas electron multiplier (GEM) detectors. These detectors work by letting particles that pass through them ionize the gas contained within the chamber, and subsequently letting said ionized gas induce an electron avalanche, resulting in an electric signal significant enough for conventional electronics to pick it up. The TPC works within a pseudo-rapidity of $|\eta| < 0.9$.

The inner tracking system (ITS) sits along the inner edge of the detector, and works alongside the TPC to improve the track resolution of higher-momentum particles. In particular, it uses silicon detectors to find primary and secondary tracks. In addition to improving the TPC's track resolution, it serves to find and identify any of the lower-momentum particles that the TPC is more likely to miss. The ITS works within a pseudo-rapidity of $|\eta| < 0.9$.

The time of flight (TOF) system is an outer shell surrounding the TPC and ITS which serves to, as the name implies, determine the time of flight of a particle from the collision point to the radius at which it sits. It uses this to determine the the mass of the particle flying through it, which is particularly important for distinguishing between particles that commonly appear out of decay chains of the heavier initial particles near the center. Namely, the TOF system is used to distinguish between protons, kaons and pions. The TOF works within a pseudo-rapidity of $|\eta| < 0.9$.[11]

The electromagnetic calorimeter (EMCal) is one of the outermost shells of ALICE, and improves its capability to detect high-energy photons and electrons. Generally, EMCal works together with the other detector systems to accurately reconstruct jet events. The EMCal works within a pseudo-rapidity of $|\eta| < 0.9$.

The muon spectrometer, as its name implies, is used to detect muons within ALICE. It is placed at a distance away from the central region, which makes its functional pseudo-rapidity range a fair bit higher compared to the previous subsystems. The muon spectrometer works within a pseudo-rapidity of $2.5 \leq \eta \leq 4.0$. Note that because it is situated on only one side of ALICE, we do not take the absolute value of the pseudo-rapidity.

3.2 Topology

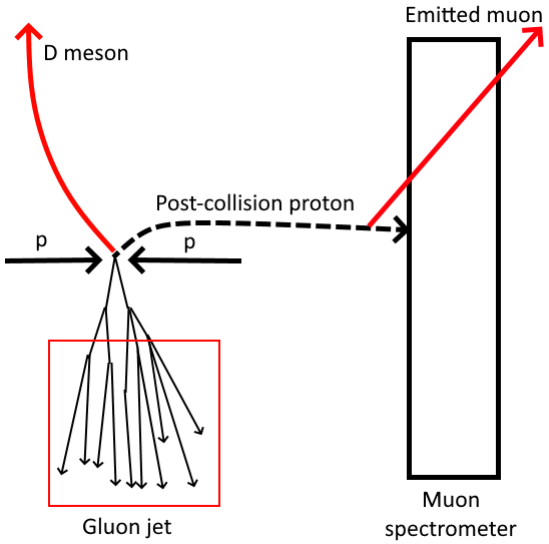

Figure 4: Schematic illustration of the proposed decay topology to study the proton intrinsic charm with the ALICE detector. After the collision of two protons, a D meson and gluon jet would be measured back-to-back at central rapidity ($|\eta| < 0.9$) using central barrel detectors, while a heavy-flavour muon would be identified using the forward muon system.

As stated, the relevant event topology we aim to investigate (displayed in Fig. 4) contains a D meson, a gluon jet, and a muon from heavy-flavour particle decays. In particular, the D meson and the gluon jet must be facing opposite directions and be contained within the central region, i.e. $|\eta| < 0.9$, such that they can be detected by their respective detector subsystems. Conversely, the muon must be in the forward region, i.e. $2.5 \leq y \leq 4.0$, such that it can be detected by the muon spectrometer. From a physics point-of-view, the aforementioned topology can materialize when one of the charm quarks from the IC pair undergoes a hard scattering with a parton (mainly a gluon at the LHC), while the other charm keeps moving at forward rapidity. This forward charm can subsequently hadronize into, for example, a Λ_c^+ baryon, and subsequently decay to emit the forward muon. Because this topology accounts for both valence charm quarks in the initial proton-proton collision (One charm has a hard scattering with a parton and forms a back-to-back gluon jet and D meson, whereas the other moves past the collision, hadronizes and decays into a forward muon), we can expect the p_T shapes of these outgoing particles to deviate from perturbative QCD expectations in accordance to the level of IC within the system.

3.2.1 D meson

The D meson is detected with the TPC, ITS and TOF systems. This project in particular looks for D^+, D^0, and $D^*(2010)^+$ mesons and their respective antiparticles, which all decay into kaons and pions before reaching the detectors because they are extremely short-lived. Namely, the mean lifetimes for the D^+, D^0, and $D^*(2010)^+$ mesons are $(1.040 \pm 0.007) \cdot 10^{-12}$ s, $(4.101 \pm 0.015) \cdot 10^{-13}$ s, and $(6.9 \pm 1.9) \cdot 10^{-21}$ s, respectively.[12] In addition to this,

these mesons all have different decay chains, of which ALICE will only be looking for specific ones. In this project, the relevant decay chains are, respectively, $D^+ \rightarrow K^- + \pi^+ + \pi^+$, $D^0 \rightarrow K^- + \pi^+$ and $D^*(2010)^+ \rightarrow D^0 + \pi^+ \rightarrow K^- + \pi^+ + \pi^+$, but plots including every single D meson will also be made as a means to add statistics. Our interest in the reconstruction of a D meson is based on the fact that it is a particle which has a charm quark as one of its valence quarks. Therefore, the meson can contain one of the two IC quarks. Indeed, the sketch in figure 4 displays this idea: one of the two IC charms interact with a gluon and produce a D meson at central rapidity, while the second charm from IC keeps flying forward, dressing in a charm hadron that then decays into a muon.

Obviously, a simple initial question would be to ask why one would not just use the D meson to investigate IC. Indeed, if we assume that IC exists and contributes to the charm production, then we should be able to measure the D meson cross-section in data, and then compare it with models including IC. This, however, is not a viable plan of approach due to the very small effect IC is expected to have in the pure cross-section. We expect effects in the order of $5 - 15\%$ in the range $100 < p_T < 200$ GeV/c. This momentum range is very high, and in data cannot grant statistical precisions better than $20 - 30\%$, making it virtually impossible to resolve an IC effect, even if it is there.[13]

3.2.2 Gluon jet

An important component of the topology we study is the presence of a gluon jet at central rapidity, opposed in ϕ to the D meson. The finding of such a combination would hint that the charm quark underwent a hard scattering with a gluon, and as a result, both were ejected at central rapidity. In ALICE, jets are reconstructed with excellent statistical precision down to very low momenta. The main detectors deputed to the jet reconstruction are ITS and TPC for charged track detection, and the EmCAL for triggering purposes. The efficiency for jet reconstruction depends wholly on the type of jet, but for charged particle jets, it ranges between 80% and 100% for track $p_T > 1$ GeV/c.

3.2.3 Muon from heavy-flavour particle decay

The statistical uncertainties for muon measurements of the spectrometer are very low, with the efficiency being as high as 98% in a wide momentum range ($0 < p_T < 30$ GeV/c).[14] The overall goal would be to tune the energy of the D meson and jet at central rapidity, while using the muon tranverse momentum spectra as a probe for IC. The work hypothesis is that if we can pick up a typical IC event topology, we are able to appreciate deviations of the p_T-dependent muon production from perturbative QCD expectations. If such a deviation were to be large enough, we would try to compare with the different IC models discussed in section 1 in order to have a first data-driven estimate of the probability of IC within the proton.

3.3 Simulation setup

The simulation itself is performed by the Stoomboot cluster located at Nikhef in Amsterdam, and consists of 3 interactive nodes and a batch cluster with 24 nodes with 32 cores each. Each

node has 256GB of RAM to work with. The largest simulations done contain two billion proton-proton collisions each, and all simulations are done at 13 TeV in the center-of-mass frame, i.e. the energy level at which the LHC is scheduled to do its next run. The simulation itself was written in C++ using the additional libraries ROOT, Pythia and LHAPDF. The purpose of each of these will now be explained.

3.3.1 ROOT

ROOT (ver. 6.22.06) is a data analysis framework, and is used to process the large amount of statistics produced by the generation of several billions of collisions. The data produced is stored as ROOT files, and subsequently manipulated with ROOT to properly display it in graphs. The functions of ROOT include rebinning the data, creating fits, using macros to compare several different ROOT files with one another, etc. This makes ROOT a fundamental part of this project, as it will be used to store the data, and to compare the data of the PDFs with IC to the PDFs without IC.

3.3.2 Pythia8

Pythia (ver. 8.3.0.3) is a C++ library that integrates with ROOT. It is lightweight and contains all of the physics required to simulate proton-proton collisions. In particular, it allows one to insert all of the initial variables into the simulation, simulate collisions using said given initial variables, and store all of the data from said collisions as ROOT files. The initial settings used in this thesis in order to produce the pp-collisions are discussed below:

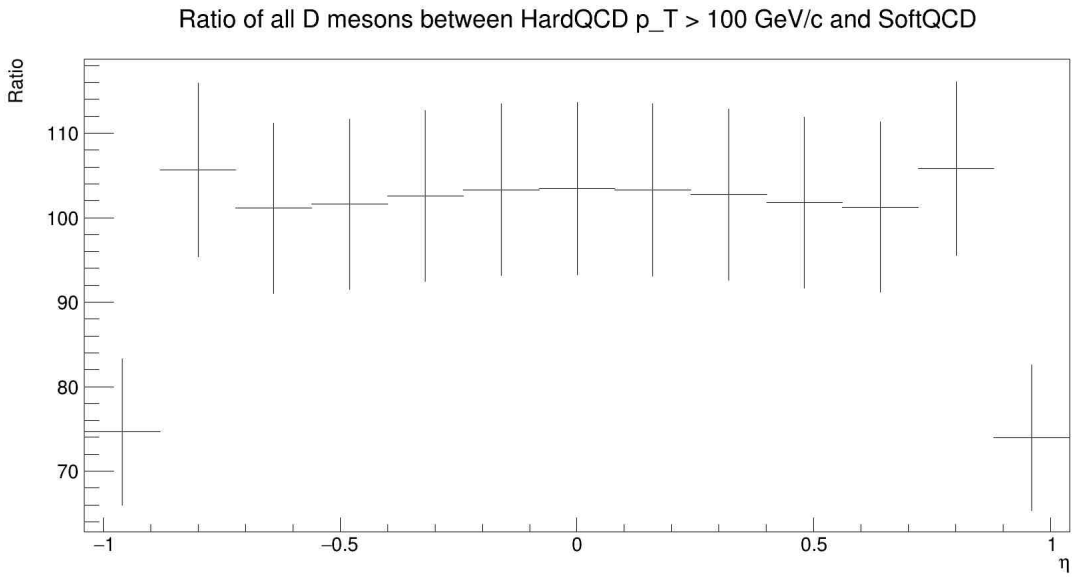

Figure 5: Ratio between the number of D mesons generated using hard QCD (minimum p_T of 100 GeV/c), and soft QCD (mimicking minimum-bias collisions). The ratio is studied as a function of the pseudorapidity and shows that the number of D mesons is increased by two orders of magnitude when using the hard QCD option.

- HardQCD:all = on. This line sets the simulation to run hard QCD processes. In addition to the change in physics, this line is necessary to make Pythia work with different PDFs (See section 3.3.3). HardQCD includes all processes above a certain p_T threshold set with the variable pTHatMin. However, it uses unregularized, divergent pQCD cross sections, meaning that it gives unreasonably large jet cross-sections if the minimum p_T is set too low. As opposed to this, SoftQCD is intended to be valid at all p_T, and is a more realistic representation of reality. The reason HardQCD is used here is so that we can set the minimum p_T of all parton interactions to a value where the effects of IC become more prevalent. This gives a larger amount of events without affecting the physics of the system. (See "PhaseSpace:pTHatMin = 100" and Fig. 5).

- Random:setSeed = on. In order to start the simulation of the collision, Pythia needs a unique number called the seed. Different seeds assure to produce a realistic set of collisions, whereas several runs with the same seed would always produce the exact same collisions. For the case of these simulations, the seeds chosen are within the range 1 to 2000, with 1 million events being simulated per seed (unless specified otherwise). This gives a total of 2 billion events.

- Tune:pp = 14. Tune:ee = 7. Pythia offers an extremely large number of initial variables to set up the collisions. These reflect the complexity of the underlying QCD processes at play. In order to produce realistic collisions, many of these parameters are tuned based on recent experimental results. Once an optimal combination is reached, Pythia saves these parameters in a so-called "tune". The tune used in this project is the Monash 2013 tune, which is especially dedicated to reproduce the experimental results on hadronization and multi-parton interactions. This tune is based on e^-e^+ and $pp/\bar{p}p$ data acquired from the large electron-positron collider (LEP) and SLAC large detector (SLD)[15]

- PhaseSpace:pTHatMin = 100. This is the line that least coincides with the reality, and is mainly in place to increase the amount of available statistics. This line sets the minimum invariant transverse momentum of each individual parton interaction to be 100 GeV/c, which means that the system is forced to contain a large amount of high-energy processes. This line in combination with the hard QCD line in particular affects the amount of D mesons within the system, which means that one should expect to need significantly more events than 2 billion in a realistic context for the same amount of relevant statistics. In order to find out how much of a difference this makes, plots comparing a soft QCD run with no minimum invariant transverse momentum to a hard QCD run with a minimum invariant transverse momentum of 100 GeV/c were made. These plots indicate that one should expect the amount of statistics to decrease by roughly two orders of magnitude, indicating that one would require roughly 200 billion events for the same amount of relevant data in a real-life context. (See figure 5)

- PDF:pSet = LHAPDF6:CT14nnloIC/x. This is the line that uses LHAPDF6 alongside Pythia8 to set the PDFs governing the physics of the collisions. Specifically, this is the line that sets the PDF to the so-called CT14nnloIC PDF set, which is a set that comes

with six different PDFs, five of which contain varying levels of IC that arise from both BHPS and SEA effects. (See section 3.3.3)

- PDF:extrapolate = on. This line extrapolates the PDFs, which are based on experimental data, to further extend into lower-energy regions where proper measurements can often not be made. This allows one to still use the PDFs in lower-energy regions.
- The remaining variables set the events to be cms (center-of-mass as opposed to a beam firing onto a stationary target) proton-proton collisions at a center-of-mass energy of 13 TeV (Coincides with scheduled LHC runs after LS2).

	No IC	BHPS1	BHPS2	SEA1	SEA2	BHPS3
Events excl. decay chain	1759856	1792182	1845451	1862175	2024563	1792222
Events incl. decay chain	157789	160330	165179	166752	181872	160293
Data remaining	8.97%	8.95%	8.95%	8.95%	8.98%	8.94%

Table 1: Number of events selected for different PDFs before and after applying the selected D meson decay channels. Roughly 9% of the events remain for all PDFs after this selection.

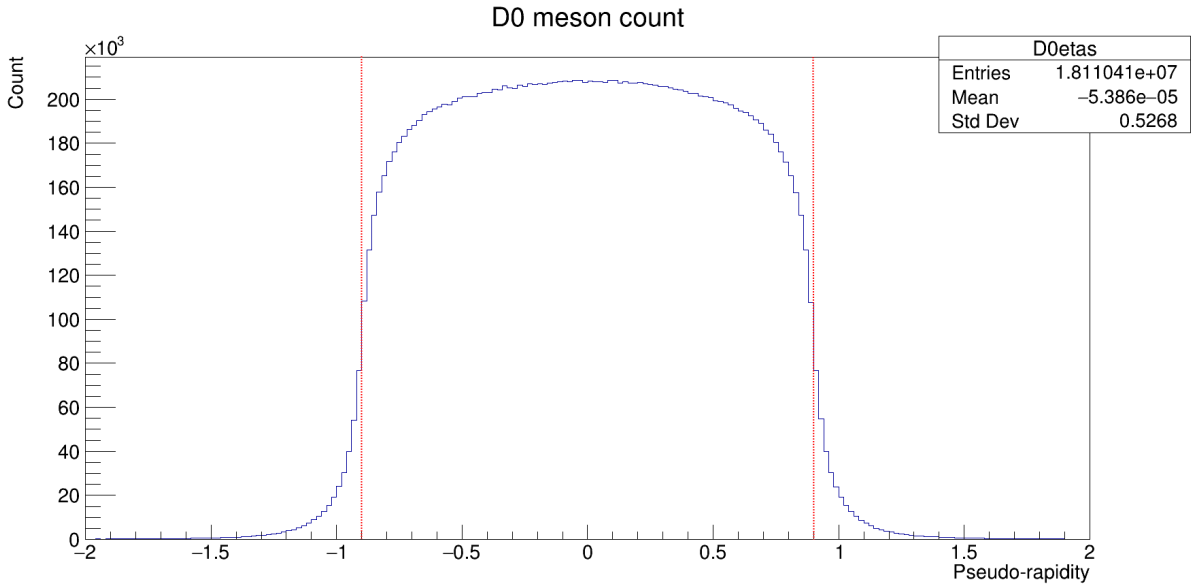

Figure 6: Decay products of D^0 mesons produced with the code. Red lines indicate the ALICE acceptance range of $|\eta| < 0.9$. This shows that roughly 4% of the D^0 meson decay products fall outside of the acceptance range, making it impossible to reconstruct the D^0 meson in ALICE.

Table 1 and figure 6 show the percentage of data that is lost when considering the previously specified decay chains rather than the mother D mesons, and the percentage of data that is lost when considering the η range of ALICE, respectively. Table 1 indicates that including these decay chains used within ALICE makes one lose roughly 91% of the data

contained within the final results. As can be seen in figure 6, the total amount of D^0 meson entries is $1.811041 \cdot 10^7$ in a set of 2 billion collisions. The entries outside of the acceptance range constitute roughly $8.0 \cdot 10^5$ of these entries, implying that in $\sim$4% of the D^0 mesons that would be in geometrical acceptance, at least one of the decay daughters would be outside of acceptance. This, during the data analysis, will result in the loss of the corresponding D^0 meson, since it will be impossible to perform the invariant mass analysis. Similar numbers can be expected for the D^+ and $D^*(2010)^+$ mesons.

In addition to all of the previously stated variables, we perform transverse momentum selections on the p_T of the gluon jet and D mesons of 20 GeV/c and 7 GeV/c, respectively. Such selections are made whilst considering the fact that charm hadrons from IC are expected to have large transverse momenta, in excess of 100 GeV/c in the central barrel region.

3.3.3 LHAPDF6

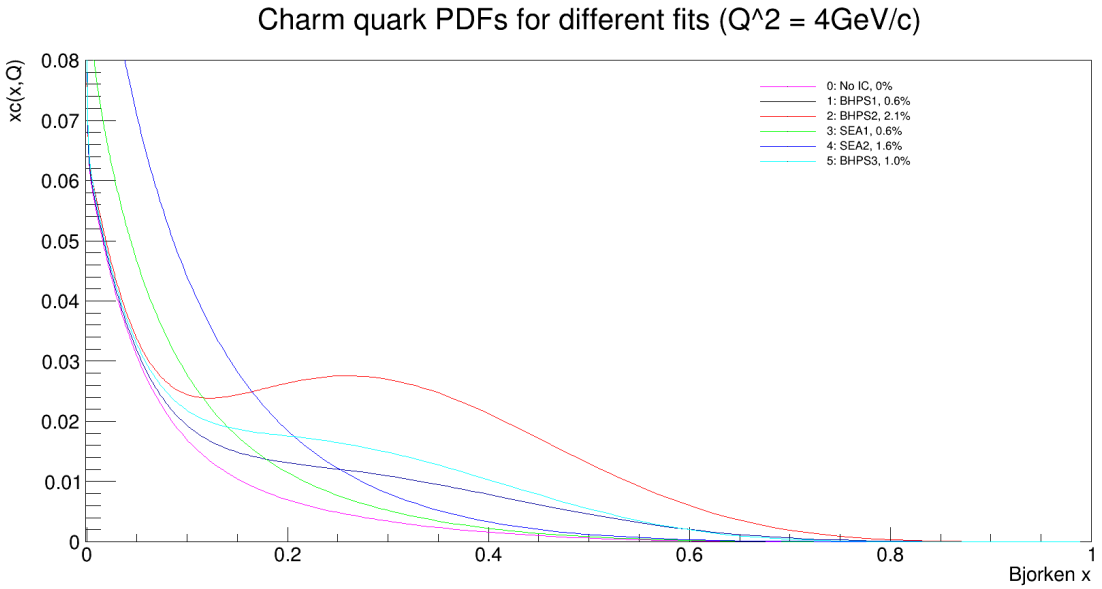

Figure 7: Charm quark PDFs with varying degrees of intrinsic charm, given at momentum transfer $Q = 2$ GeV/c. Model names and IC percentages ($\langle x \rangle_{IC}$) are given in the legend.

LHAPDF (ver. 6.3.0) is a C++ library that integrates with Pythia8 and allows one to change the PDFs that Pythia8 uses to generate events. As mentioned before, the PDF set used for this project will be the CT14nnloIC set, which contains six different PDFs. This set was produced using CTEQ-TEA (CT) analysis of QCD data, and is based on next-to-next-to-leading order (NNLO) approximations, hence the name. One of these PDFs (CT14nnloIC/0) has no IC, and thus will generally be used as a reference. The PDFs and their IC percentages are all visualized in figure 7.

Three of the PDFs are based on the BHPS model, namely CT14nnloIC/1 (BHPS1), CT14nnloIC/2 (BHPS2), and CT14nnloIC/5 (BHPS3). Although they are based on the

same model, BHPS1 and BHPS2 use cross sections acquired from the first hadron-electron ring accelerator (HERA) run, i.e. the CT14 setup, whereas BHPS3 uses run 1 and run 2 combined cross sections, i.e. the CT14HERA2 setup. They also differ in IC percentage. Namely, $\langle x \rangle_{IC} = 0.6\%$ for BHPS1, $\langle x \rangle_{IC} = 2.1\%$ for BHPS2, and $\langle x \rangle_{IC} = 1.0\%$ for BHPS3.

Two of the PDFs are based on the SEA model, namely CT14nnloIC/3 (SEA1) and CT14nnloIC/4 (SEA2). Similarly to BHPS1 and BHPS2, SEA1 and SEA2 use cross sections from the first HERA run. One can see from the PDF plots that the SEA models tend towards lower Bjorken x values compared to the BHPS models. This becomes especially evident when looking at the ratio plots (See figure 8). The IC percentages are $\langle x \rangle_{IC} = 0.6\%$ for SEA1 and $\langle x \rangle_{IC} = 1.6\%$ for SEA2.[16]

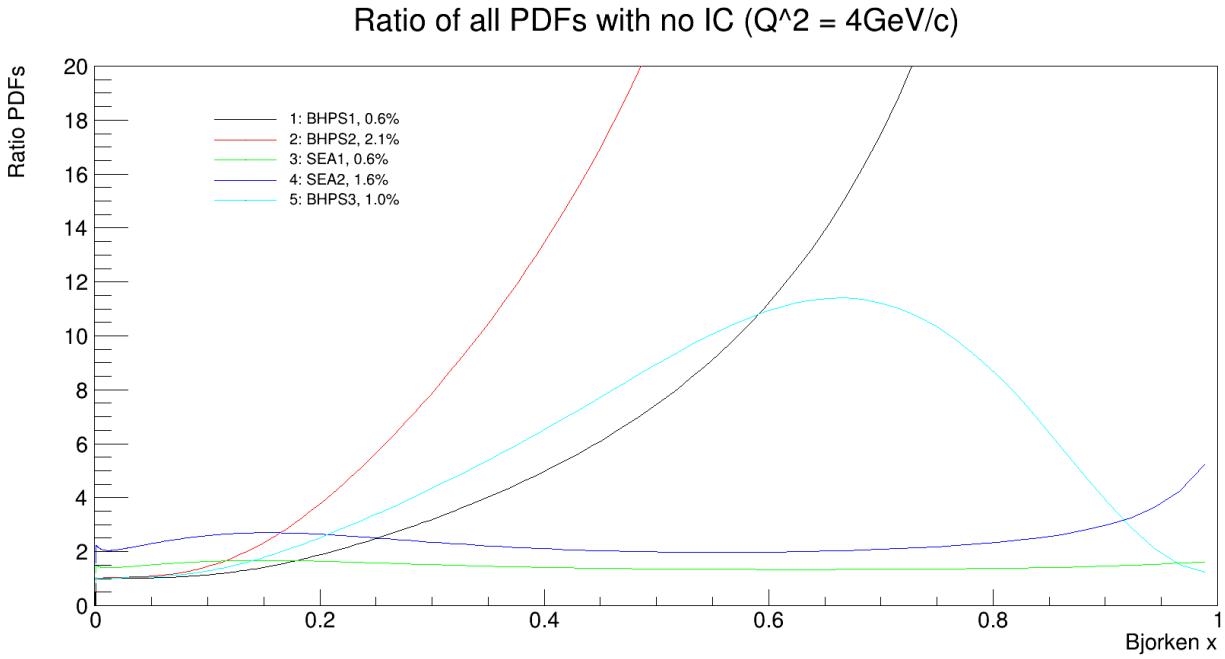

Figure 8: Ratio between charm quark PDFs with varying degrees of intrinsic charm, and a PDF with no intrinsic charm, for momentum transfer $Q = 2$ GeV/c.

In the results section, we will investigate the effects of the different PDFs on heavy-flavour hadron production, with a particular focus on the topology described earlier in this manuscript. We will assess if, by using the production of a D meson and gluon jet back-to-back at central rapidity as a trigger, we can separate the effect of IC on the forward heavy-flavour muon production, or on the eta-phi correlation between the D meson and the muon. The aim is to understand if we would be able to measure the effect with ALICE data during LHC run III (2022-2025).

4 Results and discussion

Having constructed our topology and performed the simulation, the first step of our analysis is to try to understand the effect of IC on the D meson, gluon, and forward muon. The overall idea is to try to find an observable that works as a switch for IC. In the first part of this section, we will discuss the p_T-differential production, taking into consideration the five different IC models. Such initial plots will allow us to understand the rough effect of having built our event topology. Later, we will discuss the possibility to tune the momentum scale of a member of the topology (namely the D meson and the gluon) in order to enhance the effect of IC on the third member (the muon). Finally, we will investigate the correlation in eta-phi of the D meson and the muon in order to try to understand if charm from IC events would correlate differently than charm produced perturbatively.

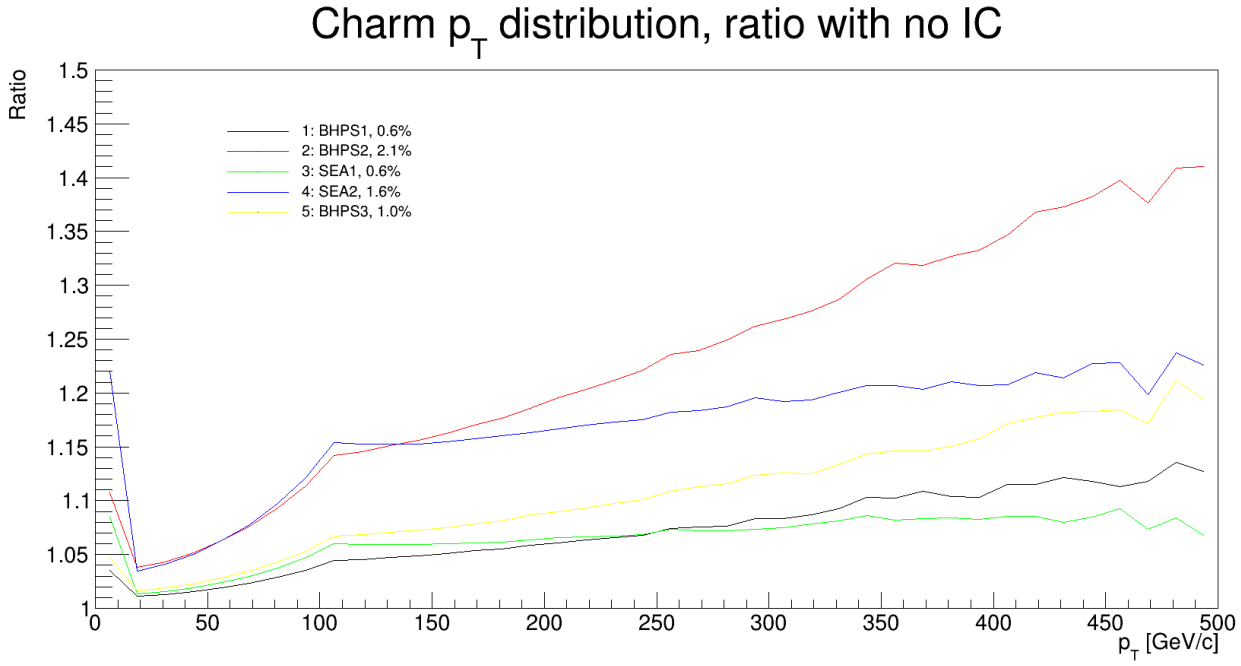

Figure 9: Amount of charm quarks within the system for the different PDFs, given as a ratio to the PDF without IC. This shows that BHPS models overtake SEA models with similar IC percentages at higher p_T ranges. (Error bars omitted due to very large amount of statistics)

As can be seen in figure 9, the SEA models have a tendency to have a larger charm ratio (charm quark amount ratio with the model with no IC) than their respective BHPS models in the lower p_T ranges, with the SEA2 model being roughly as high as the BHPS2 model at $p_T = 100$ GeV/c, despite having a lower IC percentage, and the SEA1 model being higher than the BHPS1 model at $p_T = 100$ GeV/c, despite having the same IC percentage. This makes sense because, as was seen in figure 8, the SEA models tend to have their peak ratio values at lower Bjorken x compared to the BHPS models, with the SEA models becoming particularly relevant around $x = 0.15$. However, the BHPS models quickly take over the SEA models at $x > 0.2$. These higher Bjorken x values coincide with higher p_T values, explaining

how BHPS2 overtakes SEA2 at $p_T = 130$ GeV/c.

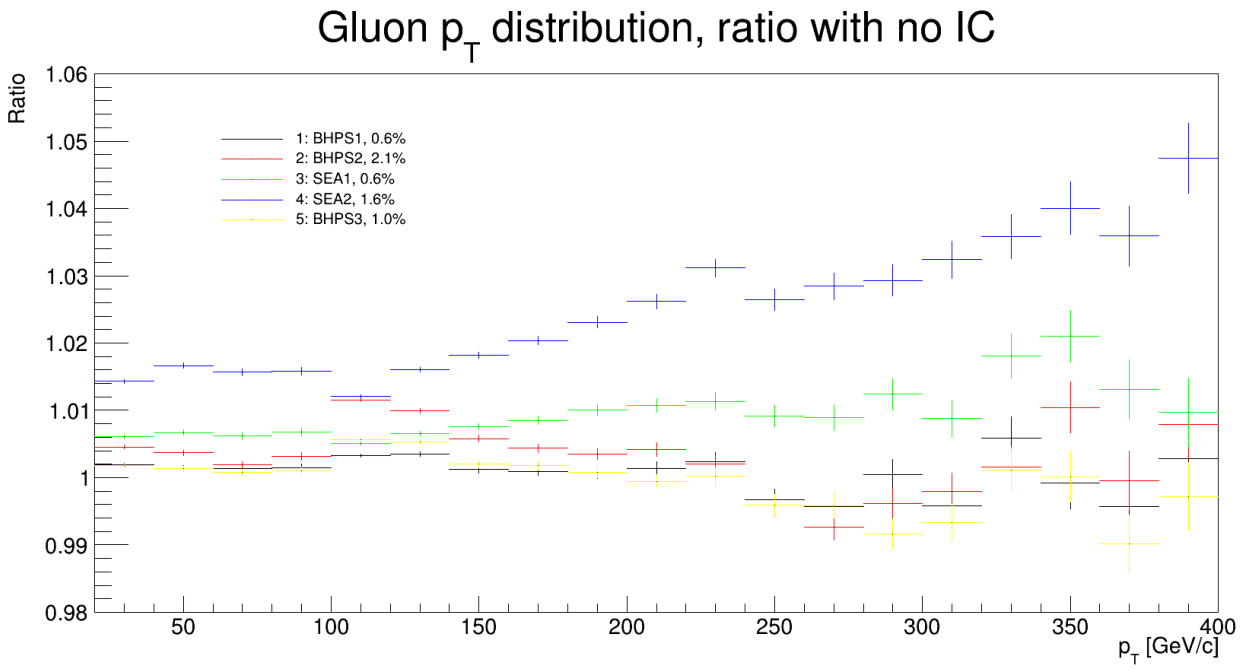

Figure 10: Amount of gluons within the system for the different PDFs as a ratio to the PDF without IC, showing that SEA models favour gluon production. In this plot, muons are not yet looked for.

In addition to the difference in ratio between the different models, one can note that the data has a strange discontinuity at $p_T = 100$ GeV/c. This occurs due to the imposed minimum p_T value per parton interaction, which gives the system a strong tendency to contain partons at and above this p_T level. Despite the fact that this increases the amount of data at these higher energy values, it does not fundamentally change the physics of the system, making it a valid strategy to decrease uncertainties within the simulation (See section 3.3.2).

As can be seen in figure 10, the amount of gluons in a two-billion run does not necessarily depend on the percentage of IC of the PDF. Rather, the SEA models tend to have a larger amount of gluons produced than their respective BHPS models, which makes sense considering SEA models produce $c\bar{c}$-pairs by means of a gluon component (See section 2.2). It can also be seen in figure 11 that considering the entire topology immediately affects the ratios by rather significant amounts. This indicates that our topology is able by itself to preferentially select IC events, and that the high-pseudorapidity muon is a likely candidate for a trigger particle.

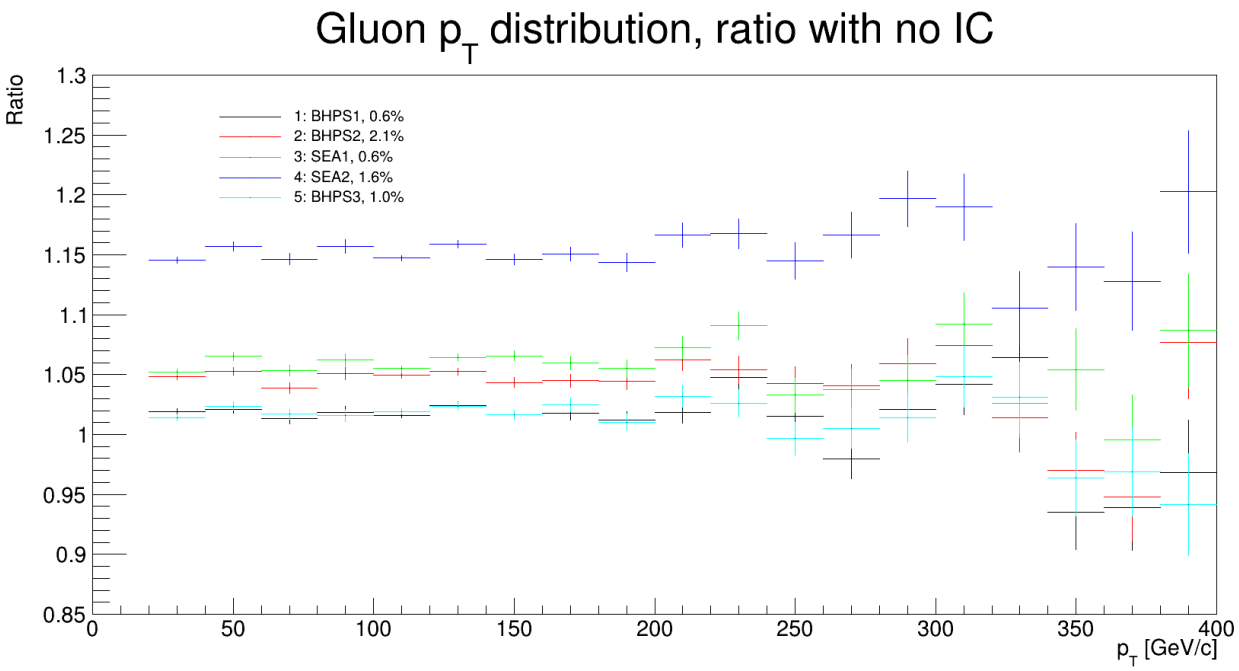

Figure 11: All events (findings of the full topology) given as a gluon p_T distribution (ratio to the PDF with no IC). In this plot and all subsequent plots (unless stated otherwise), the full topology is considered, which increases the ratio for all models.

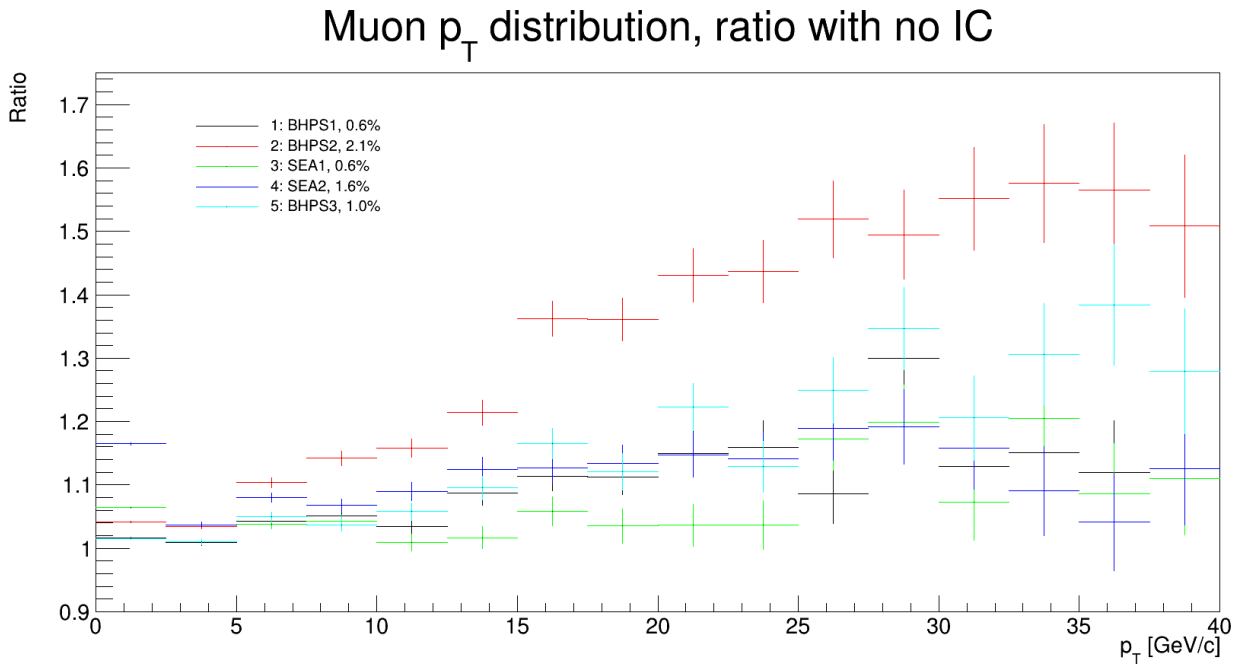

Figure 12: Muon p_T (GeV/c) distributions for PDFs with varying degrees of IC, given as a ratio to the PDF with no IC.

The amount of muons seems to be affected directly by the amount of IC within the PDF (see figure 12) significantly more than the gluons. This is as expected, since they stem di-

rectly from charm hadron decays. Additionally, the muons produced with BHPS models seem to be affected more than their respective SEA models in almost all p_T bins. In fact, the SEA models only overtake the BHPS models when $p_T \leq 5$ GeV/c. These large ratios indicate that there is a possibility to use muons to research IC, and more plots should be made to see if this increase can be further amplified, or used to amplify the ratio in other particles.

The final bare p_T distribution number ratio plot is that of the D mesons within the system (see figure 13). In this plot, note that the SEA2 model seems to contain more D mesons than all other models. In general, all the models except for the aforementioned SEA2 show effects on the production of the D mesons in the order of a few % below a p_T of 200 GeV/c. Above such thresholds, the IC effect starts to pick up. However, D mesons are reasonable rare objects, and the ALICE detector, in the decade spanning 2011 to 2021, was able to investigate D meson production until a p_T of 100 GeV/c at best. The statistical uncertainties above 50 GeV/c become sizeable, reaching the order of $20 - 40\%$. As discussed in section 3.2.1, the ALICE collaboration plans to acquire a factor 10 more statistics in the coming years. While this is a large increase, it will surely not be enough to detect D mesons in excess of $p_T = 200$ GeV/c. Therefore, while it is interesting to see the effect of IC on their production probability in this p_T range, this observable alone will almost surely not help with an experimental measurement.

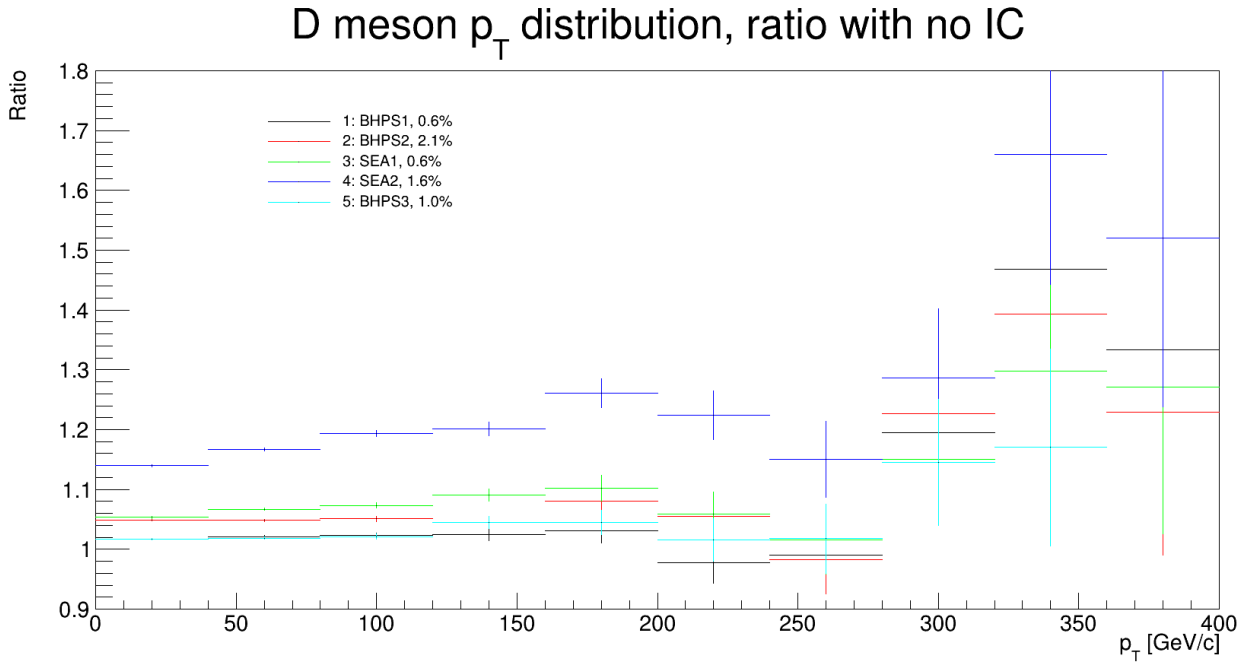

Figure 13: D meson p_T (GeV/c) distributions for PDFs with varying degrees of IC, given as a ratio to the PDF with no IC.

Although the most promising particle within the topology appears to be the muon, which is the particle with the highest pseudorapidity within the system, it is worth investigating

if larger η differences between the gluons and D mesons can pinpoint the IC effect in a clearer way. In addition, it is mandatory to investigate if, by restricting the p_T scale of one of the members of the topology, we can control the size of the IC effect on the other members.

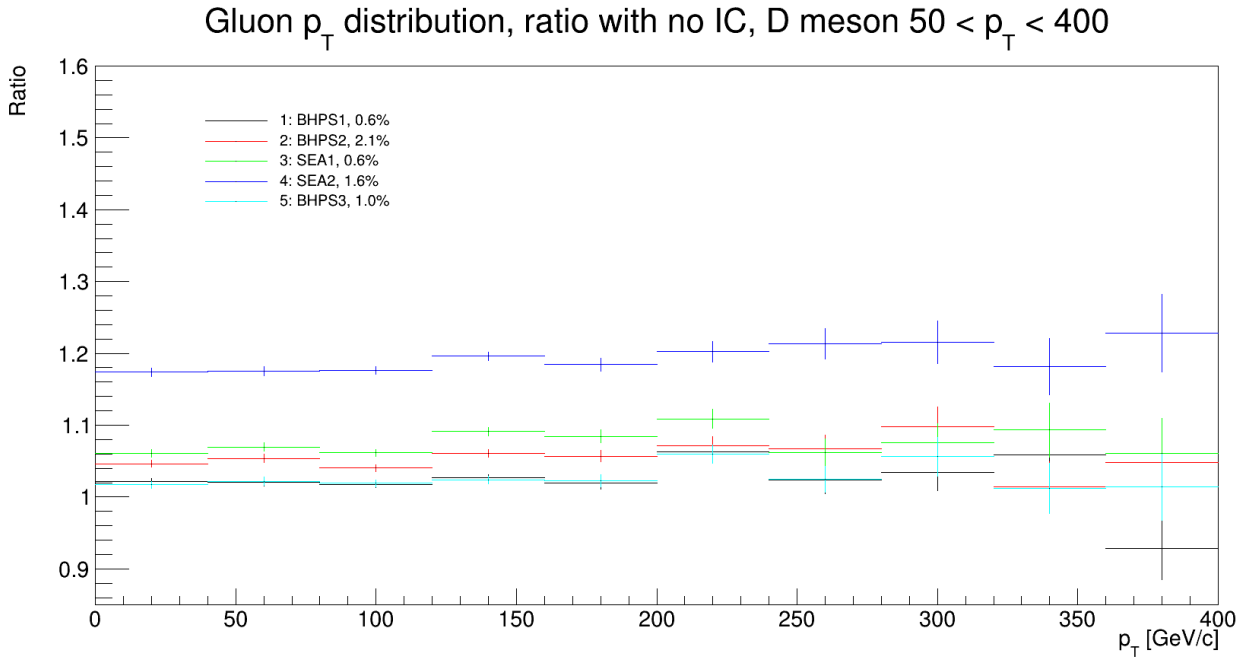

Figure 14: Gluon p_T (GeV/c) distributions for PDFs with varying degrees of IC, given as a ratio to the PDF with no IC. D meson p_T restricted between 50 GeV/c and 400 GeV/c.

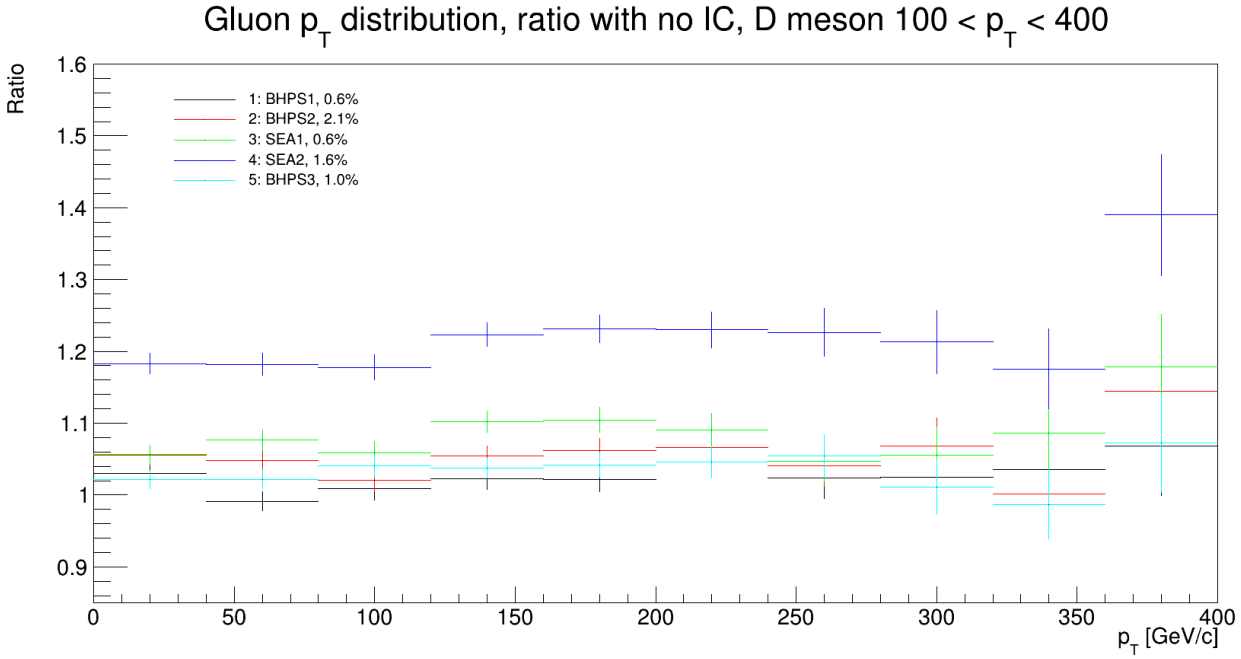

Figure 15: Gluon p_T (GeV/c) distributions for PDFs with varying degrees of IC, given as a ratio to the PDF with no IC. D meson p_T restricted between 100 GeV/c and 400 GeV/c.

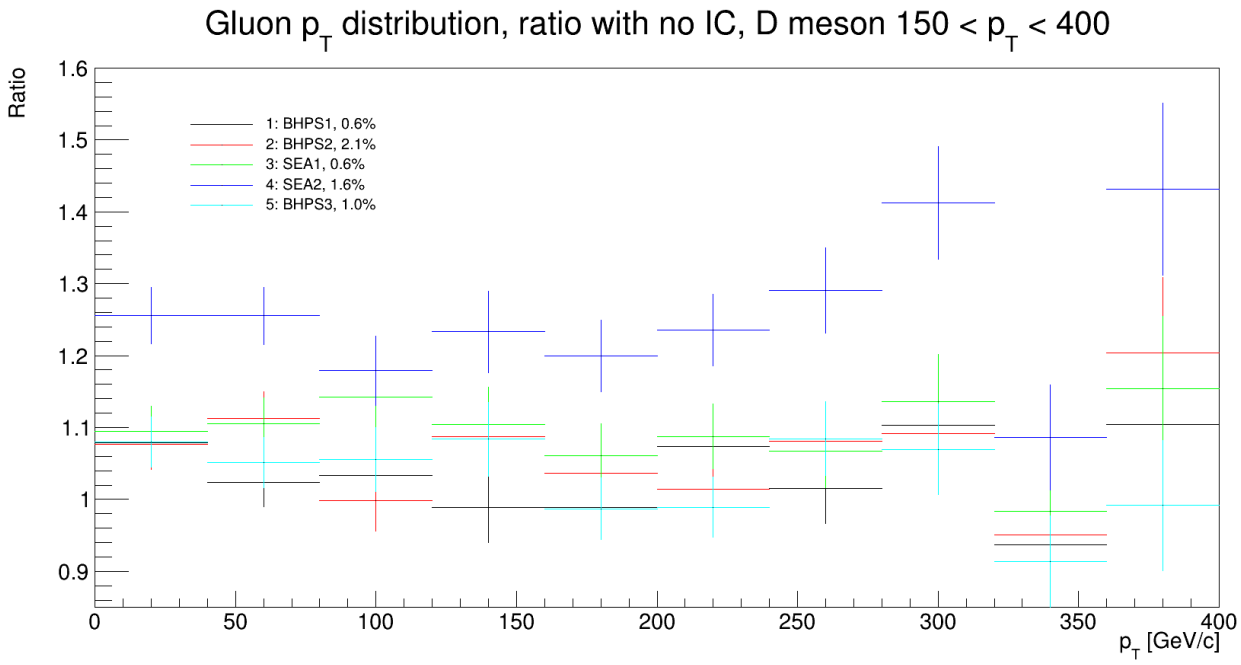

Figure 16: Gluon p_T (GeV/c) distributions for PDFs with varying degrees of IC, given as a ratio to the PDF with no IC. D meson p_T restricted between 150 GeV/c and 400 GeV/c.

Figures 14, 15 and 16 highlight the effect of increasing D meson p_T bins on the gluon jets. These indicate that models with IC, in particular SEA models, are affected by restrictions of the minimum p_T of the D mesons. In particular combinations of high p_T values of both the gluon and the D meson seem to lead to a much more pronounced IC effect.

As can be seen in table 2, the SEA2 model appears to be particularly affected by the D meson p_T bins, with its ratios increasing from 5 to 12%. That being said, the BHPS models seem to not be affected nearly as much, with increases in the order of several percentages being the most prevalent. Although gluon jets can be reconstructed rather accurately, the differences here are rather small. Additionally, the fact that BHPS models are mostly unaffected does not bode well for this method.

In addition to the different p_T ranges, it is worth investigating if correlation peaks occur at particular pseudorapidity (η) or angle (ϕ [π rad]) differences between the D meson and gluon jet. In figures 17-22, plots displaying distributions for these differences are displayed. What is particularly notable is that the $\Delta\phi$ distributions in particular are mostly unchanged for all p_T bins.

Gluon: $0 < p_T < 100$	PDF:	BHPS1	BHPS2	SEA1	SEA2	BHPS3
D meson p_T:	$0 < p_T < 400$	+2%	+5%	+6%	+15%	+2%
	$50 < p_T < 400$	N/A	+5%	+6%	+17%	+2%
	$100 < p_T < 400$	+1%	+5%	+6%	+18%	+2%
	$150 < p_T < 400$	+5%	+8%	+11%	+25%	+6%

Gluon: $100 < p_T < 200$	PDF:	BHPS1	BHPS2	SEA1	SEA2	BHPS3
D meson p_T:	$0 < p_T < 400$	+2%	+5%	+6%	+15%	+2%
	$50 < p_T < 400$	+2%	+5%	+8%	+19%	+2%
	$100 < p_T < 400$	+2%	+5%	+10%	+22%	+4%
	$150 < p_T < 400$	-1%	+5%	+9%	+20%	+3%

Gluon: $200 < p_T < 300$	PDF:	BHPS1	BHPS2	SEA1	SEA2	BHPS3
D meson p_T:	$0 < p_T < 400$	+2%	+5%	+6%	+17%	+2%
	$50 < p_T < 400$	N/A	+8%	+9%	+21%	+5%
	$100 < p_T < 400$	N/A	+6%	+7%	+23%	+5%
	$150 < p_T < 400$	+7%	+6%	+8%	+29%	+4%

Table 2: Tables displaying the percentage difference (compared to no IC) in the number of events of each PDF in the specified gluon and D meson p_T bins.

$3.6 < \Delta\phi < 3.8$	PDF:	BHPS1	BHPS2	SEA1	SEA2	BHPS3
Gluon p_T:	$0 < p_T < 200$	+2%	+5%	+6%	+15%	+2%
	$10 < p_T < 200$	N/A	+5%	+6%	+16%	+2%
	$20 < p_T < 200$	+5%	+13%	+9%	+18%	+7%

Table 3: Table displaying the percentage difference (compared to no IC) in the number of events of each PDF in the specified $\Delta\phi$ range and gluon p_T bins.

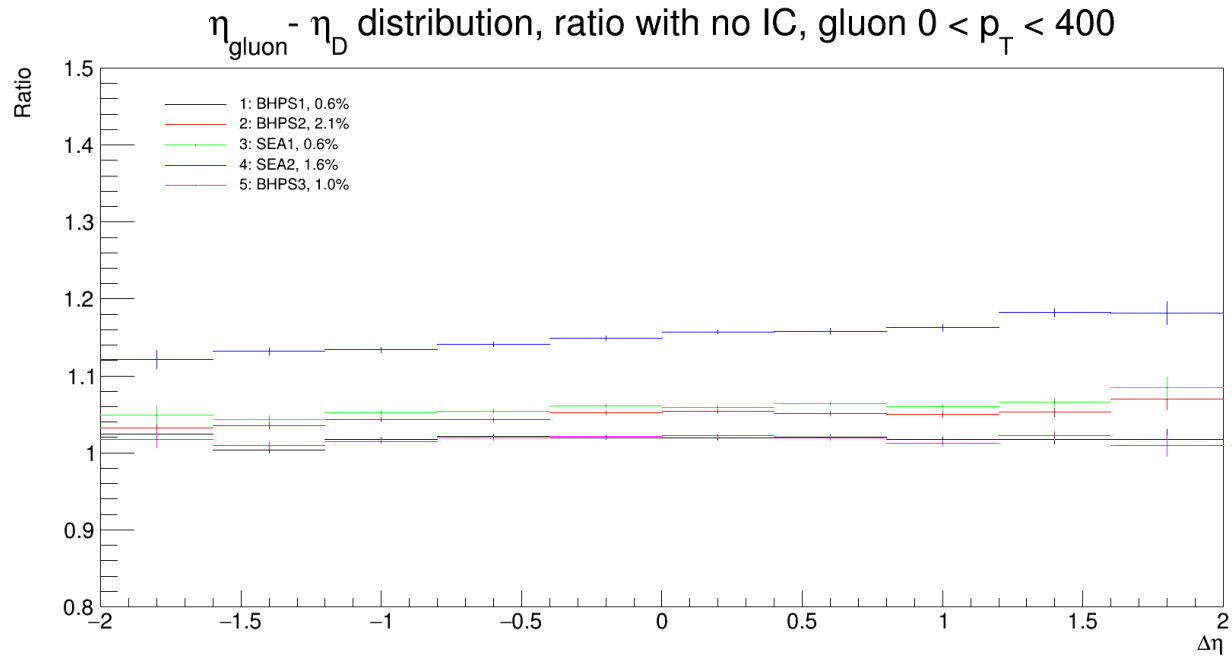

Figure 17: Distribution of the $\Delta\eta$ between the gluon and D meson for PDFs with varying levels of IC, given as a ratio to a PDF with no IC. Gluon p_T restricted between 0 GeV/c and 400 GeV/c.

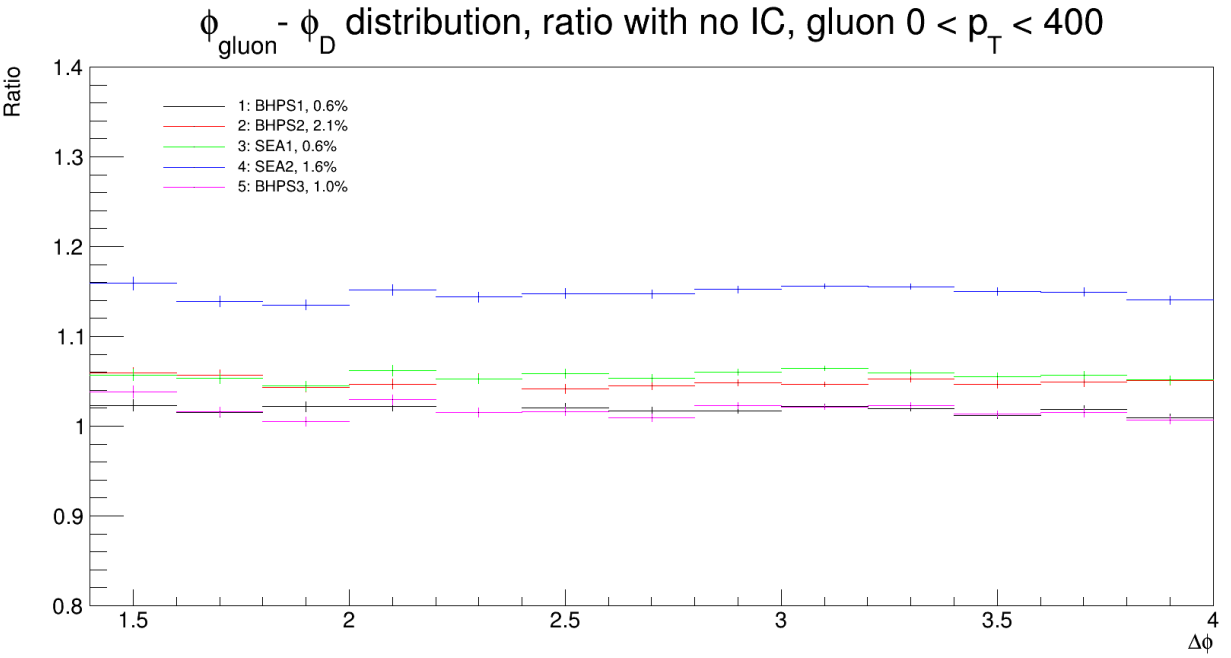

Figure 18: Distribution of the $\Delta\phi$ between the gluon and D meson for PDFs with varying levels of IC, given as a ratio to a PDF with no IC. Gluon p_T restricted between 0 GeV/c and 400 GeV/c.

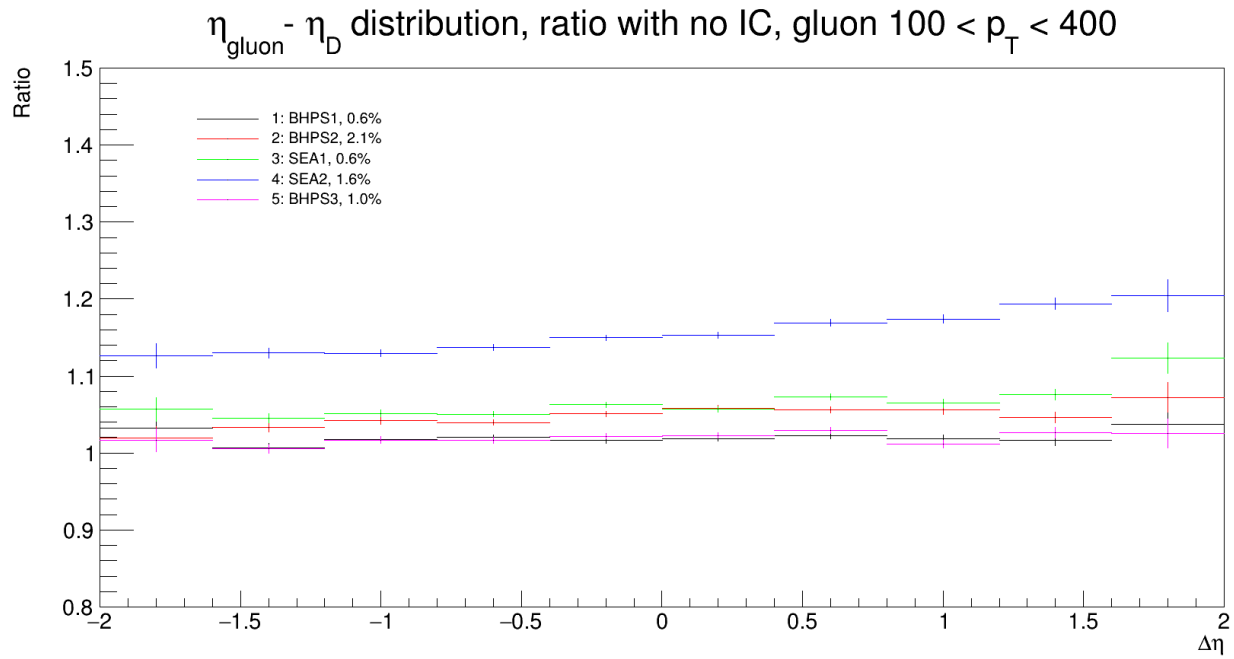

Figure 19: Distribution of the $\Delta\eta$ between the gluon and D meson for PDFs with varying levels of IC, given as a ratio to a PDF with no IC. Gluon p_T restricted between 100 GeV/c and 400 GeV/c.

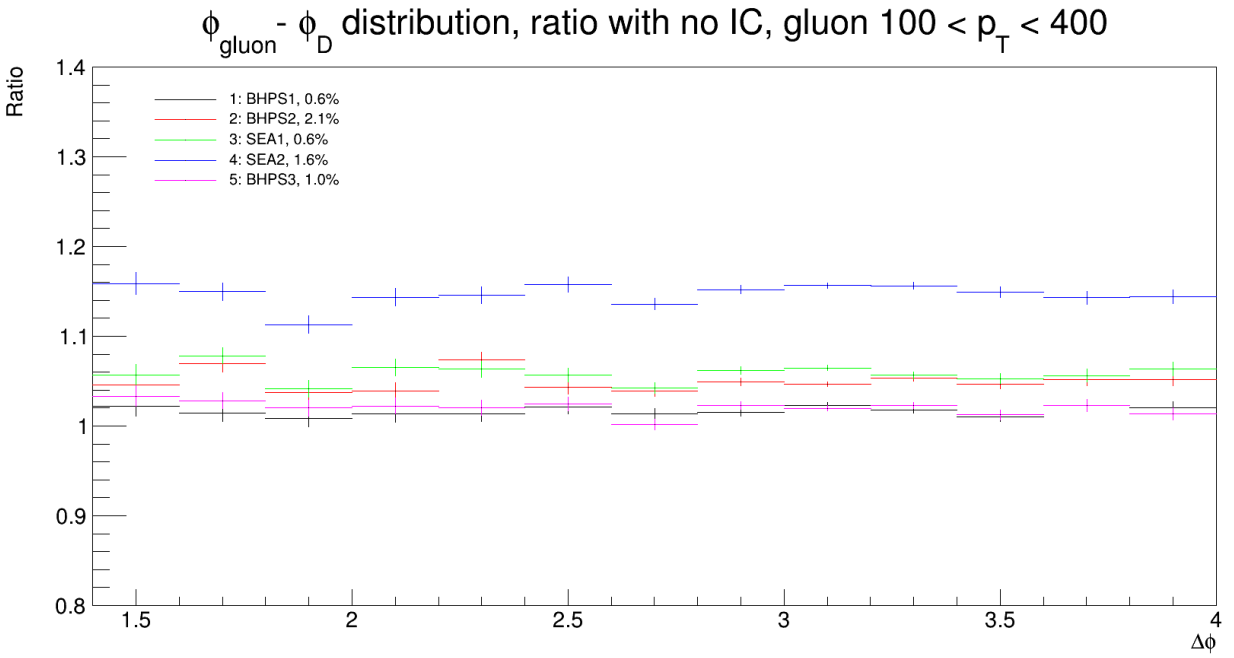

Figure 20: Distribution of the $\Delta\phi$ between the gluon and D meson for PDFs with varying levels of IC, given as a ratio to a PDF with no IC. Gluon p_T restricted between 100 GeV/c and 400 GeV/c.

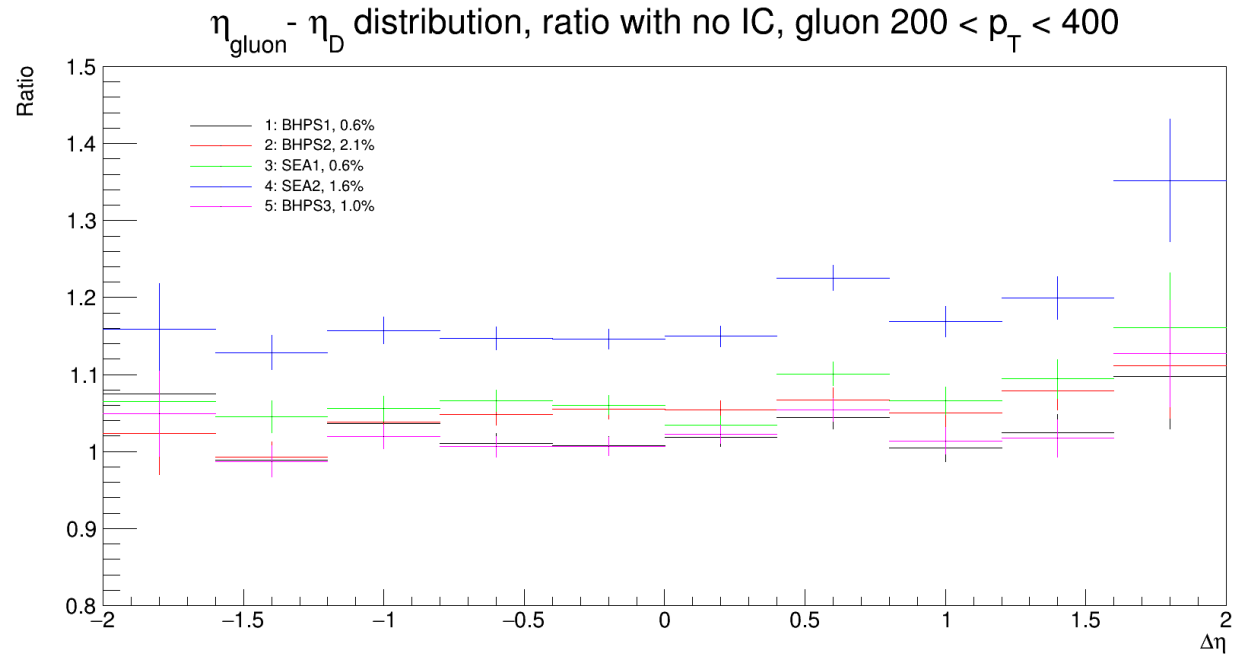

Figure 21: Distribution of the $\Delta\eta$ between the gluon and D meson for PDFs with varying levels of IC, given as a ratio to a PDF with no IC. Gluon p_T restricted between 200 GeV/c and 400 GeV/c.

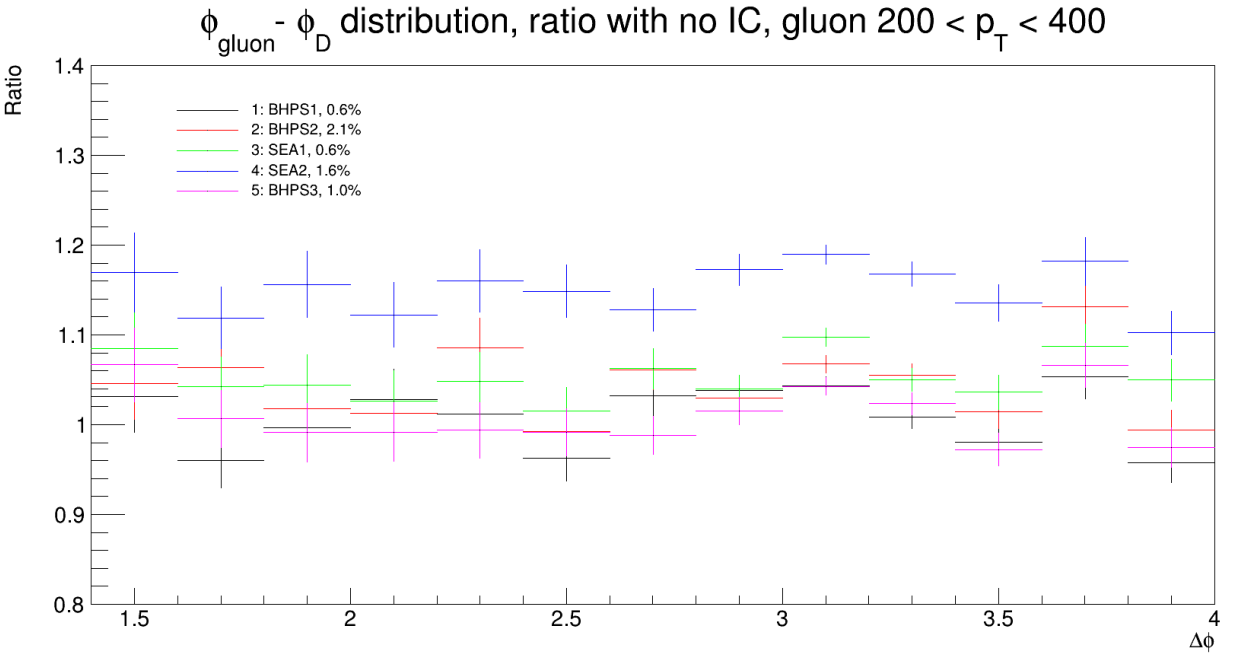

Figure 22: Distribution of the $\Delta\phi$ between the gluon and D meson for PDFs with varying levels of IC, given as a ratio to a PDF with no IC. Gluon p_T restricted between 200 GeV/c and 400 GeV/c.

As opposed to the $\Delta\phi$ plots, the $\Delta\eta$ distributions display a more steady increase, in particular for the SEA models. Most notably, the region of highest $\Delta\eta$, so $3.8 < \Delta\eta < 4.0$, seems to be affected by the increased minimum gluon p_T. This makes sense, because as stated in section 2.2, systems involving IC tend towards higher Feynman x values, and thus higher pseudorapidities.

Considering the striking increase of the event ratio for high forward muon p_T displayed in figure 12, the gluon and D meson p_T distributions will be remade, now with limited muon p_T ranges. This will show if the distributions of other particles within the topology are affected by the muons to such an extent that high-p_T muons can be used as a trigger for IC. Figures 23-26 display the effect of limiting the muon p_T on the gluon jet, and figures 27-30 do so for the D meson. Tables 4 and 5 contain the data displayed in these plots for BHPS2, which is the PDF with the highest percentage of IC, and also the PDF that appears to be the most affected by the muon p_T restrictions.

	Gluon p_T:	20-40	40-60	60-80	80-100	100-120
Muon p_T:	$0 < p_T < 200$	+5%	+5%	+4%	+5%	+5%
	$10 < p_T < 200$	+32%	+36%	+31%	+28%	+23%
	$20 < p_T < 200$	+54%	+56%	+68%	+51%	+38%
	$30 < p_T < 200$	+58%	+65%	+101%	+58%	+50%

	Gluon p_T:	120-140	140-160	160-180	180-200
Muon p_T:	$0 < p_T < 200$	+5%	+4%	+4%	+4%
	$10 < p_T < 200$	+30%	+23%	+26%	+30%
	$20 < p_T < 200$	+38%	+40%	+90%	+76%
	$30 < p_T < 200$	+60%	+65%	+118%	+79%

Table 4: Table displaying the percentage difference (compared to no IC) in the number of events for the PDF BHPS2 in the specified gluon p_T ranges (columns) and muon p_T ranges (rows). See figures 23-26 for full data.

	D meson p_T:	0-40	40-80	80-120	120-160	160-200	200-240
Muon p_T:	$0 < p_T < 200$	+5%	+5%	+5%	N/A	+8%	+6%
	$10 < p_T < 200$	+33%	+26%	+19%	+20%	+12%	-16%
	$20 < p_T < 200$	+58%	+44%	+29%	+20%	+41%	N/A
	$30 < p_T < 200$	+74%	+56%	+30%	+17%	+36%	+17%

Table 5: Table displaying the percentage difference (compared to no IC) in the number of events for the PDF BHPS2 in the specified D meson p_T ranges (columns) and muon p_T ranges (rows). See figures 27-30 for full data. Note that some of the high-p_T points have rather large uncertainties.

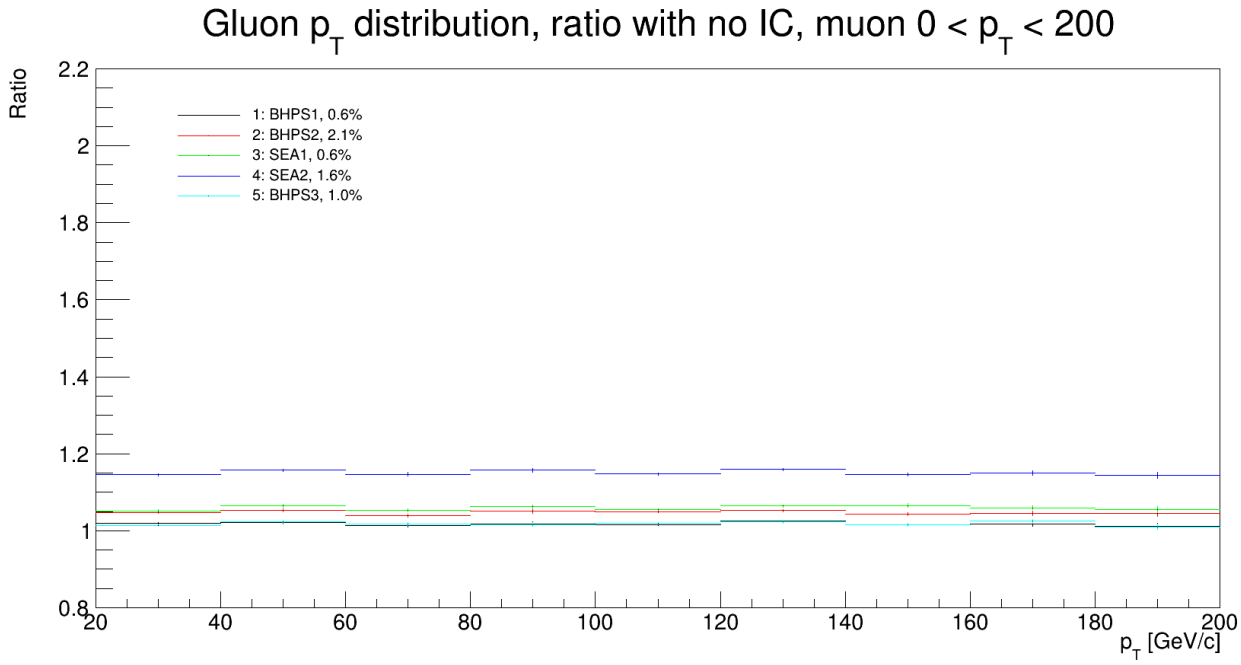

Figure 23: Gluon p_T (GeV/c) distributions for PDFs with varying degrees of IC, given as a ratio to a PDF with no IC. Muon p_T restricted between 0 GeV/c and 200 GeV/c.

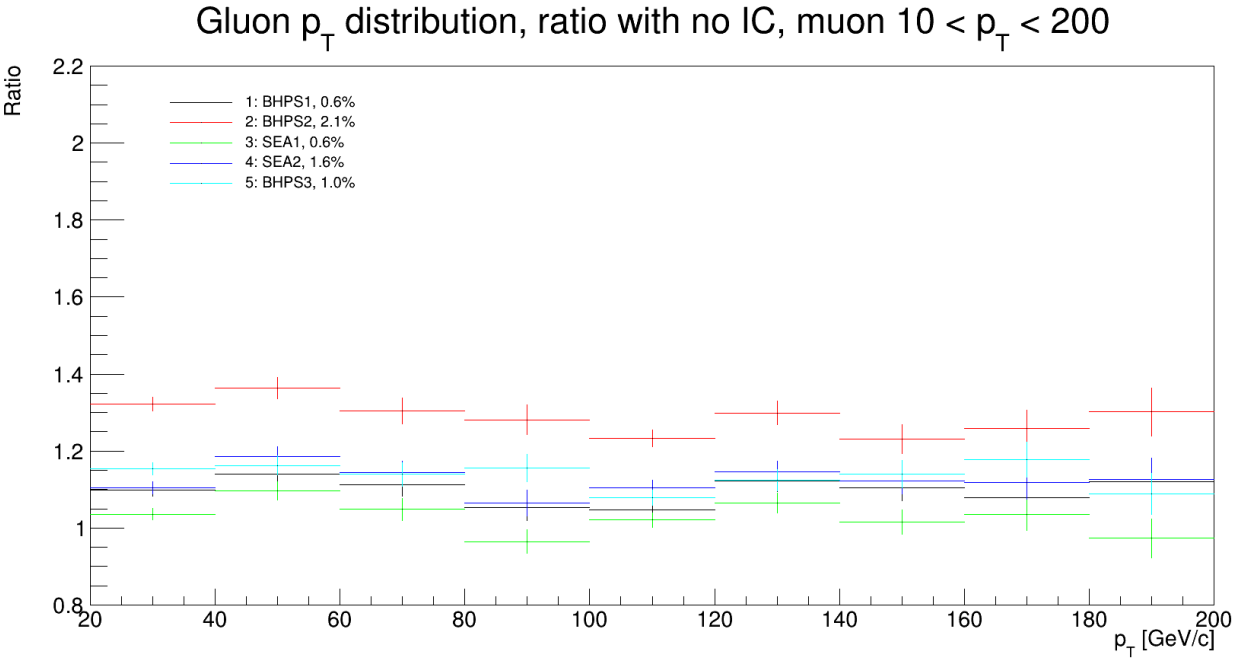

Figure 24: Gluon p_T (GeV/c) distributions for PDFs with varying degrees of IC, given as a ratio to a PDF with no IC. Muon p_T restricted between 10 GeV/c and 200 GeV/c.

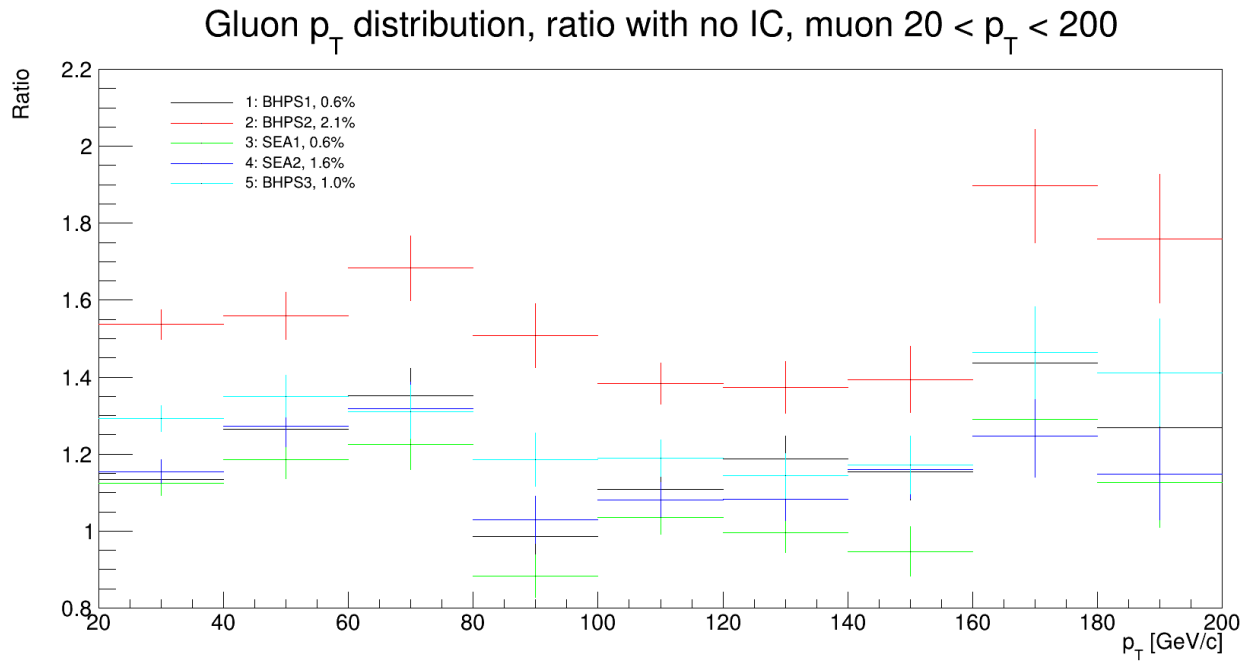

Figure 25: Gluon p_T (GeV/c) distributions for PDFs with varying degrees of IC, given as a ratio to a PDF with no IC. Muon p_T restricted between 20 GeV/c and 200 GeV/c.

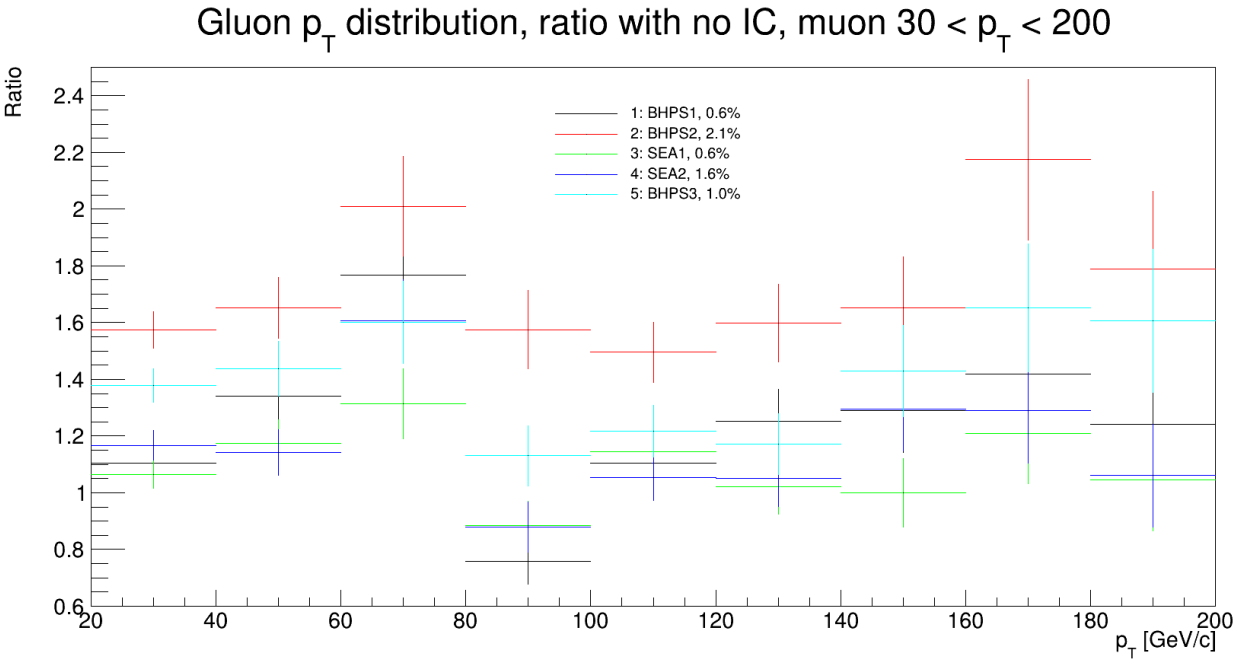

Figure 26: Gluon p_T (GeV/c) distributions for PDFs with varying degrees of IC, given as a ratio to a PDF with no IC. Muon p_T restricted between 30 GeV/c and 200 GeV/c.

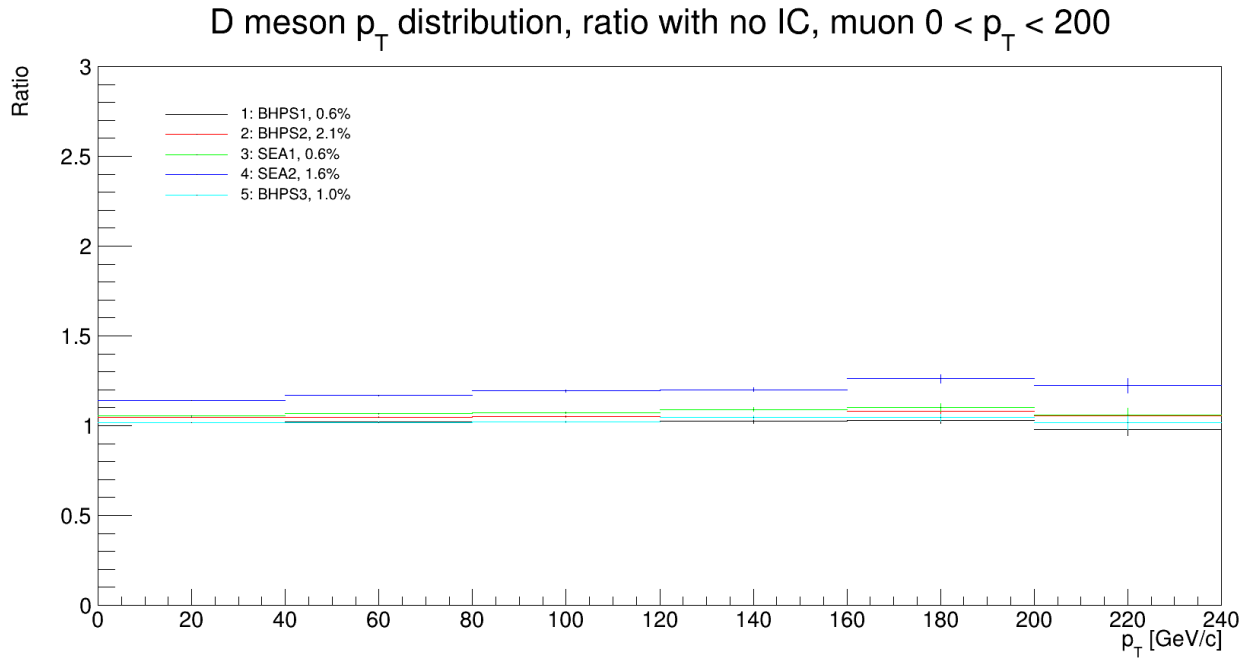

Figure 27: D meson p_T (GeV/c) distributions for PDFs with varying degrees of IC, given as a ratio to a PDF with no IC. Muon p_T restricted between 0 GeV/c and 200 GeV/c.

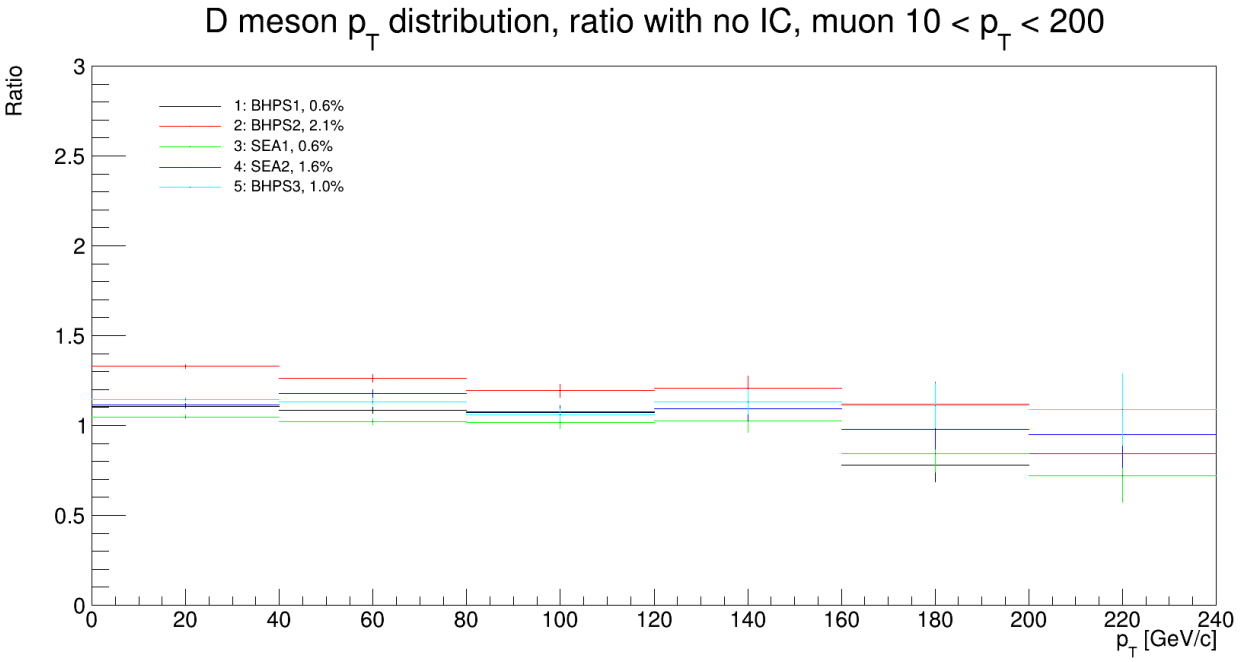

Figure 28: D meson p_T (GeV/c) distributions for PDFs with varying degrees of IC, given as a ratio to a PDF with no IC. Muon p_T restricted between 10 GeV/c and 200 GeV/c.

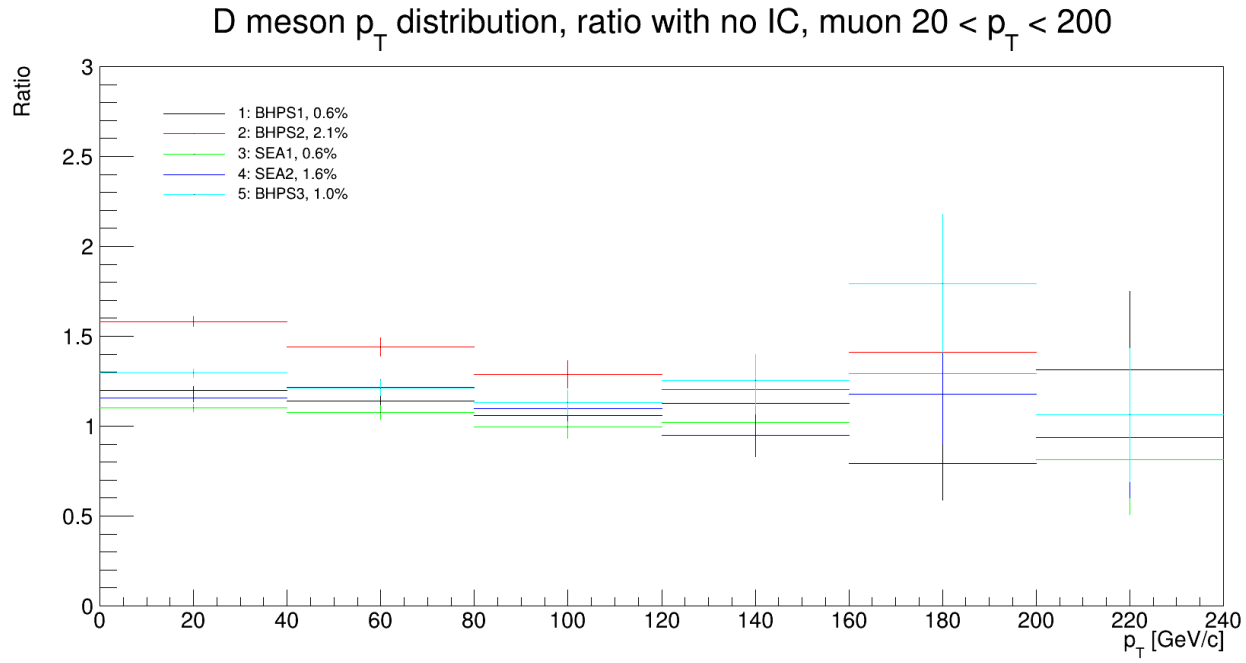

Figure 29: D meson p_T (GeV/c) distributions for PDFs with varying degrees of IC, given as a ratio to a PDF with no IC. Muon p_T restricted between 20 GeV/c and 200 GeV/c.

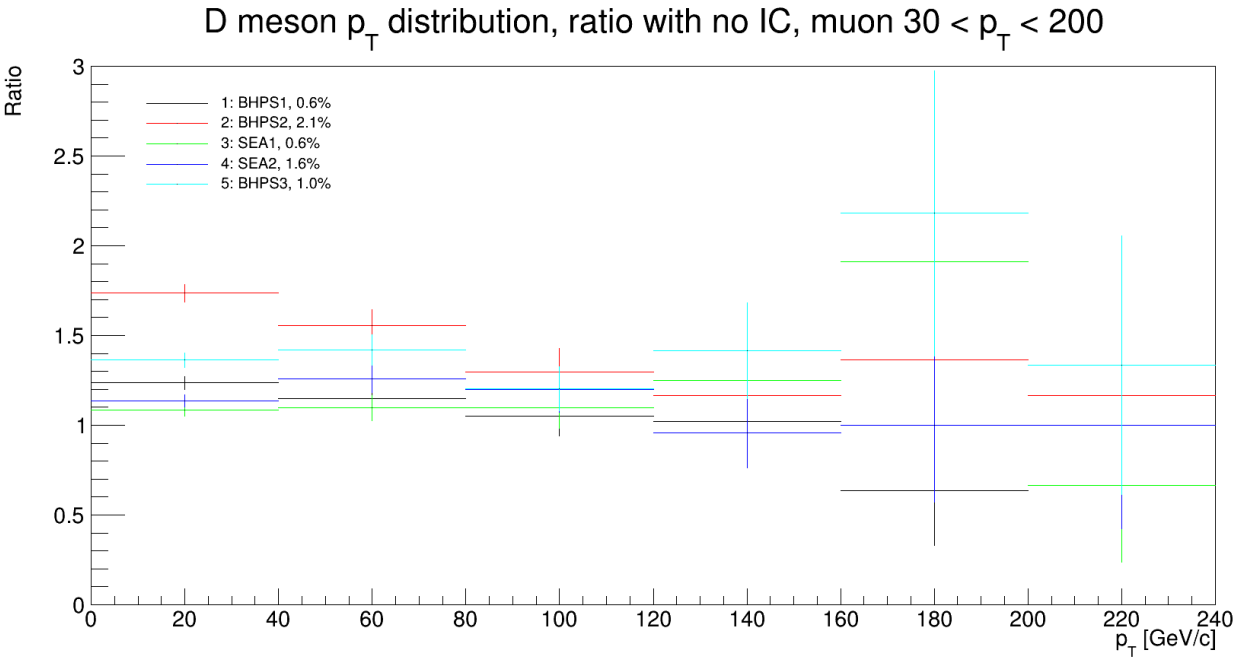

Figure 30: D meson p_T (GeV/c) distributions for PDFs with varying degrees of IC, given as a ratio to a PDF with no IC. Muon p_T restricted between 30 GeV/c and 200 GeV/c.

There are several notable features that can be observed in figures 23-30. First of all, note that the presence of IC results in a noticeable deviation of the gluon jet production from perturbative QCD expectations. Some of the peaks in the gluon distributions more than double the amount of events, which is very promising. There is also a very clear correlation between the minimum muon p_T and the ratio in the gluon distributions.

For the D meson distributions, a very interesting feature that can be noted is that, as the minimum muon p_T increases, the difference in ratio between the D meson p_T bins gets larger and larger. However, contrary to what one might expect, these ratios seem to favour lower D meson p_T bins. Indeed, all muon p_T ranges where a minimum above 0 GeV/c is set, display this feature.

Considering the seeming effect of muon and D meson p_T bins on IC, figure 31 displays a $\Delta\eta$ plot between the D meson and muon using a combination of low D meson and high muon p_Ts. This plot displays that, given a combination of the correct p_T bins, IC seems to favour large $\Delta\eta$ values significantly. Note that the forward muon will always have an η between 2.5 and 4.0, so the final two bins of figure 31 indicate that a forward muon with a particularly high η, and a D meson with a particularly low η are seemingly preferred in systems with a larger percentage of IC.

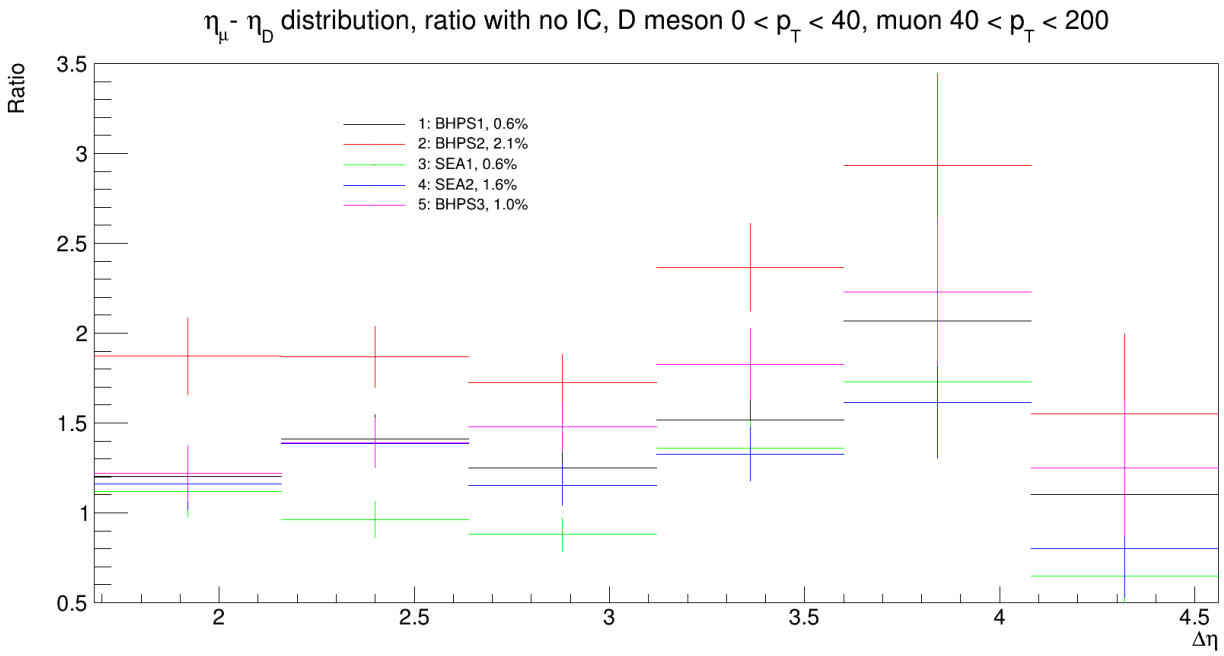

Figure 31: Distribution of the $\Delta\eta$ between the muon and D meson for PDFs with varying degrees of IC, given as a ratio to a PDF with no IC. D meson p_T restricted between 0 GeV/c and 40 GeV/c, muon p_T restricted between 40 GeV/c and 200 GeV/c.

5 Conclusions and future outlook

Before concluding anything about the data, it is fair to point out that we used methods that enhance the charm production in the simulation in order to achieve a good amount of statistics in the limited time frame of this project, with the main difference being the setting of a minimum p_T for hard parton scattering. The removal of the minimum p_T per parton interaction would already decrease the amount of statistics by a factor 100. Not to mention the decay chain considerations, which decrease the amount of available D mesons by another order of magnitude. Considering these two implementations already result in a decrease in data of three orders of magnitude, it is mandatory to point out that, in order to achieve in real data analysis results similar to those of the simulation, we would need at least 2 trillion collisions. However, ALICE is to acquire in the order of 100 billion pp events' worth of data in the scheduled LHC Run III. Therefore, it might still take a considerable amount of time, possibly until 2030, to have the statistics to perform the first experimental measurement of the intrinsic charm probability in the proton.

The simulation study we performed, however, is very promising and points at the possibility to study the intrinsic charm probability via its effect on the production of forward heavy-flavour decay muons. From our results (see Fig. 12), it seems clear that a measurement implementing our topology would be able to resolve IC in BHPS models if the IC probability in the proton is above 1%. Indeed, in such models, we predict an effect of $40 - 80\%$ on the shape of the forward muons at about $20 - 30$ GeV/c in p_T. Such effects can be measured easily by ALICE. Moreover, it is clear that once the IC probability goes below 1%, and especially for SEA models, the situation is less promising. We can see that in those cases, the overall effect in the same p_T interval reduces to the order of $10 - 15\%$. Such a level is likely to be a problem whilst analyzing data due to statistical and systematic uncertainties. However, given a large enough deviation from the effects in these p_T intervals, it would allow for the refutation of the SEA models.

In addition to confirming that the implementation of the topology is effective, our results (see Table 2) show that limiting the p_T range of just the gluon jet is an inadequate measure, resulting in increases in the order of several percentages at best in BHPS2, which is the model with the highest IC percentage at 2.1%. Moreover, Figs. 17-22 show that considering the η and ϕ differences between the D meson and gluon jet do not ameliorate these increases at all.

However, Tables 4-5 display clearly that combining the previously mentioned increases in forward muon p_T with limited p_T ranges in at least the D meson allows one to further magnify the ratios. Table 4 indicates that combining muon p_T restrictions with gluon p_T restrictions is not particularly fruitful, with increases of $50 - 60\%$ with gluon p_T range $20 - 120$ GeV/c and $60 - 80\%$ with gluon p_T range $120 - 200$ GeV/c, but seemingly random spikes of $+101\%$ and $+118\%$ for gluon p_T ranges $60 - 80$ GeV/c and $160 - 180$ GeV/c, respectively. However, Table 5 shows us that, given a high minimum muon p_T of 30 GeV/c, lower D meson p_T ranges of 0-40 are favoured significantly, giving a ratio increase of 74% in BHPS2 as opposed to the significantly smaller $17 - 36\%$ in the higher p_T range $80 - 240$ GeV/c. This is, indeed, a proof that our forking hypothesis is correct. The topology we studied is

characteristic of intrinsic charm events, and the transverse momentum of the D meson allows us to switch on and off the intrinsic charm effect on the forward muons' p_T distribution shape.

Finally, Fig. 31 displays that one can utilize the previously observed increase when combining a low D meson p_T range with a high minimum muon p_T value in combination with the pseudo-rapidity difference between the two to acquire increases ranging from +60% to +200%, with the SEA models being least affected. From this, we can draw the conclusion that IC events are particularly prevalent in the highest muon pseudo-rapidity ranges.

Given the very promising nature of the study, and especially the result of figure 31, it would be worth it to consider different combinations of variables in the future. For example, it would be interesting to investigate further if, by varying the p_T ranges of the gluon jet and/or the D meson, we can better control the IC effect on the $\Delta\eta$ of the D meson and muon. Our preliminary results suggest so, and this would allow us to have two observables ($\Delta\eta$ and muon p_T) that allow us to study IC. Additionally, it would be useful to make individual η plots for both the muons and the D mesons to see which particle contributes to what extent to the spike at $3.6 < \Delta\eta < 4.1$ in figure 31. One final plot that was not made due to time constraints, but would be interesting to see, is one where figure 31 is re-made with constraints on the p_T ranges of all of the three particles within the topology.

6 Laymen summary

It is common knowledge that the matter we are made of is made of atoms. Looking at them in detail, it turns out that the atoms themselves are made of smaller particles: protons and neutrons being held together by the strong nuclear force constituting the nucleus of the atom, and electrons orbiting this nucleus under the effect of the electromagnetic force. Finally, even protons and neutrons are composite objects made of quarks and gluons. Quarks and their interactions in particular are mediated by a force called the strong force. We describe this strong force using so-called quantum chromodynamics (QCD), which is a type of quantum field theory. In this theory, the strong force is mediated by particles called gluons. All experimental data so far confirms this picture, and proves that QCD is an effective representation of what happens in nature.

We know that, in general, the protons and neutrons that make up all of our atoms have very specific combinations of valence (bound) quarks. For example, protons always have two up-quarks and one down-quark, whereas neutrons always have one up-quark and two down-quarks. However, nature is rather complex at the smallest scale, and there are effects at play that allow protons and neutrons to occasionally contain more. They can do this in several different ways, but most of the ways that can properly be described are so-called 'perturbative' mechanisms.

As opposed to perturbative QCD, which is more easily-described, there are also mechanisms that we know less about that are non-perturbative. Intrinsic charm is one of these. For one, it is a long-term intrinsic feature of every proton, and it essentially allows a proton to appear in states where it does not just have two up-quarks and a down-quark, but also a pair of charm-quarks. From theory, we can predict that the intrinsic component becomes significantly larger than the perturbative one under specific circumstances. Most notably, in high-energy proton collisions, when the particles that come out are angled in roughly the same direction as the protons that collide with one another (i.e. a more parallel trajectory rather than a perpendicular one), intrinsic components are more likely to appear than perturbative ones, whereas perpendicular trajectories favour perturbative contributions.

This difference in regions wherein both contributions tend to show up allows us to test, to some extent, which of the two mechanisms we are dealing with. However, the difference is usually so small that one needs to use refined techniques, like the one proposed in this manuscript, to enhance the intrinsic charm component.

In this thesis, a novel technique to enhance the intrinsic charm component by triggering on heavy-flavoured (heavy-flavoured: composite particles that contain a charm-quark or beauty-quark, which are heavier flavours of up-quarks and down-quarks, respectively) particles is investigated. The idea is that one searches for an outgoing D meson (combination of a charm-quark, and some other anti-quark) and a so-called gluon jet, the two of which are back-to-back and lie roughly in the plane perpendicular to the proton beam direction, and a muon from heavy-flavour hadron (hadron: composite particle made of quarks) decays that flies in the direction of the proton beam (forward direction). In this thesis, we proved that

the aforementioned topology is effective in selecting intrinsic charm, and it gives the ALICE experiment a real possibility to measure this effect in the coming years. In particular, it seems feasible to limit the transverse momentum range of the D meson to control the intrinsic charm effect on the transverse momentum-dependent production of the muon.

References

[1] Manuel Mussini. Measurement of low p_T D^0 meson production cross section at CDF II. 2021.

[2] Michiel Botje. Lecture notes Particle Physics II. Nikhef Science Park, 12 2013.

[3] John C. Collins, Davison E. Soper, and George Sterman. Factorization of hard processes in QCD. 2004.

[4] M. Cacciari, M. Greco, and P. Nason. The p_t Spectrum in Heavy-Flavour Hadroproduction. 1998.

[5] Jon Pumplin. Light-Cone Models for Intrinsic Charm and Bottom. 2005.

[6] S. J. Brodsky, C. Peterson, and N. Sakai. Intrinsic heavy-quark states. *Phys. Rev. D*, 23:2745–2757, Jun 1981.

[7] Rafal Maciula and Antoni Szczurek. Intrinsic charm in the nucleon and charm production at large rapidities in collinear, hybrid and k_t-factorization approaches. 2020.

[8] A. V. Giannini, V. P. Goncalves, and F. S. Navarra. Intrinsic charm contribution to the prompt atmospheric neutrino flux. 2018.

[9] A. Szczurek and Rafal Maciula. $D\bar{D}$ Asymmetry at Low and High Energies and Possible Consequences for Prompt Atmospheric Neutrinos. *Acta Physica Polonica B*, 49, 03 2018.

[10] J. Alme et al. The ALICE TPC, a large 3-dimensional tracking device with fast readout for ultra-high multiplicity events. *Nuclear Instruments and Methods in Physics Research Section A: Accelerators, Spectrometers, Detectors and Associated Equipment*, 622(1):316–367, 2010.

[11] A. Akindinov et al. Particle identification with the ALICE TOF detector at very high particle multiplicity. *Eur. Phys. J. C*, 32S1:165–177, 2004.

[12] P.A. Zyla et al. Review of Particle Physics. *PTEP*, 2020(8):083C01, 2020.

[13] ALICE Collaboration. Measurement of D-meson production at mid-rapidity in pp collisions at $\sqrt{\mathbf{s}} = \mathbf{7}$ TeV. 2017.

[14] Christian Finck and Alice Muon Spectrometer collaboration. The muon spectrometer of the ALICE. *Journal of Physics: Conference Series*, 50:397–401, nov 2006.

[15] Peter Skands, Stefano Carrazza, and Juan Rojo. Tuning pythia 8.1: the monash 2013 tune. 2014.

[16] Tie-Jiun Hou, Sayipjamal Dulat, Jun Gao, Marco Guzzi, Joey Huston, Pavel Nadolsky, Carl Schmidt, Jan Winter, Keping Xie, and C. P. Yuan. CT14 Intrinsic Charm Parton Distribution Functions from CTEQ-TEA Global Analysis. 2017.